






# ObjectCompose: Evaluating Resilience of Vision-Based Models on Object-to-Background Compositional Changes

Hashmat Shadab Malik<sup>\*1</sup>, Muhammad Huzaifa<sup>\*1</sup>, Muzammal Naseer<sup>1</sup>,  
Salman Khan<sup>1,2</sup>, and Fahad Shahbaz Khan<sup>1,3</sup>

<sup>1</sup> Mohamed bin Zayed University of AI

<sup>2</sup> Australian National University

<sup>3</sup> Linköping University

hashmat.malik@mbzuai.ac.ae, muhammad.huzaifa@mbzuai.ac.ae,  
muzammal.naseer@mbzuai.ac.ae, salman.khan@mbzuai.ac.ae,  
fahad.khan@mbzuai.ac.ae

**Abstract.** Given the large-scale multi-modal training of recent vision-based models and their generalization capabilities, understanding the extent of their robustness is critical for their real-world deployment. In this work, our goal is to evaluate the resilience of current vision-based models against diverse object-to-background context variations. The majority of robustness evaluation methods have introduced synthetic datasets to induce changes to object characteristics (viewpoints, scale, color) or utilized image transformation techniques (adversarial changes, common corruptions) on real images to simulate shifts in distributions. Recent works have explored leveraging large language models and diffusion models to generate changes in the background. However, these methods either lack in offering control over the changes to be made or distort the object semantics, making them unsuitable for the task. Our method, on the other hand, can induce diverse object-to-background changes while preserving the original semantics and appearance of the object. To achieve this goal, we harness the generative capabilities of text-to-image, image-to-text, and image-to-segment models to automatically generate a broad spectrum of object-to-background changes. We induce both natural and adversarial background changes by either modifying the textual prompts or optimizing the latents and textual embedding of text-to-image models. This allows us to quantify the role of background context in understanding the robustness and generalization of deep neural networks. We produce various versions of standard vision datasets (ImageNet, COCO), incorporating either diverse and realistic backgrounds into the images or introducing color, texture, and adversarial changes in the background. We conduct thorough experimentation and provide an in-depth analysis of the robustness of vision-based models against object-to-background context variations across different tasks. Our code is available at <https://github.com/Muhammad-Huzaifaa/ObjectCompose>

**Keywords:** Robustness · Adversarial · Foundation Models

<sup>\*</sup> Equal contribution.

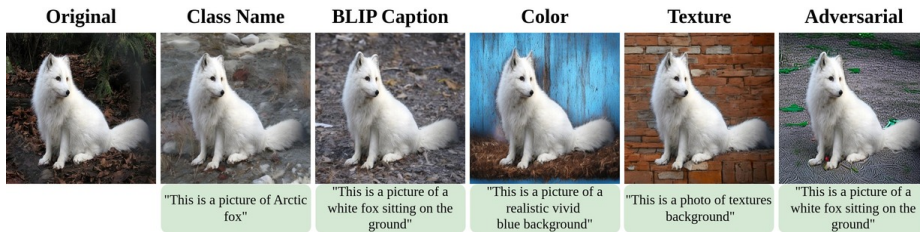


**Fig. 1:** The image-to-background variations by our approach. Each column in the figure represents a specific background generated through the corresponding prompt mentioned below of each image.

## 1 Introduction

Deep learning-based vision models have achieved significant improvement in diverse vision tasks. However, the performance on static held-out datasets does not capture the diversity of different object background compositions present in the real world. In order for these models to be deployed in security-critical applications, analyzing the robustness of these models under diverse changes in the distribution of the data is crucial. Previous works have shown that vision models are vulnerable to a variety of image alterations, including common corruptions (e.g., snow, fog, blur) [21, 41], domain shifts (e.g., paintings, sketches, cartoons) [19, 20], and changes in viewpoint (e.g., pose, shape, orientation) [3, 5, 27]. Additionally, carefully designed perturbations can be added to images to create adversarial examples that are imperceptible to humans but can fool the decision-making of vision models [16, 58].

Several approaches have been proposed to improve the out-of-distribution robustness of vision models. To achieve adversarial robustness, models are typically trained on adversarial examples [40], and various augmentation policies were proposed to improve non-adversarial robustness of models [8, 20, 62, 63]. More recently, the computer vision field has seen the emergence of large-scale pre-training of both vision [31, 44] and vision-language models [33, 46, 57]. Trained on large-scale datasets and multiple modalities, these models demonstrate promising performance on non-adversarial distribution shifts. Consequently, several works [30, 65] have adapted these models for downstream tasks by utilizing learnable prompts to preserve the rich feature space learned during pre-training.

To evaluate the vision-based models on different distribution shifts, numerous benchmarking datasets, comprising either synthetic or altered real images have been proposed. While synthetic datasets [5, 15, 28] offer more control over desired changes (background, shape, size, viewpoint), most of them capture only simple shape objects within a controlled environment. On the other hand, several studies [21, 41] employ coarse-grained image manipulations on the available ImageNet dataset [10]. However, the coarse-grained transformations used do not encompass the diverse changes that can be induced in real images.



Recent works [35,45] have focused on leveraging existing foundational models to forge new ways to evaluate the resilience of uni/multi-modal vision models. In [45], large language models and text-to-image diffusion models are used for generating diverse semantic changes in real images. However, their method relies on prompt-to-prompt editing [23], allowing only the modification of specific words in the prompt for making changes. Furthermore, due to absence of strong guidance between the object and background during image editing, it often leads to distortion in the object semantics. In [35], diffusion models are used for background editing in real images, and ImageNet-E(diting) dataset is introduced for benchmarking. However, their primary focus is on varying the texture complexity of background by introducing a frequency-based loss for guidance in the denoising process of diffusion model. This imposes limitations on the type of background-compositions that can be achieved. In this work, we address the above limitations and develop a framework for investigating the resilience of vision-based models against diverse object-to-background changes. We accomplish this task by utilising the complementary strengths of current image-to-text [33], image-to-segment [31] and text-to-image [24,47] foundational models to create a framework that is significantly more adept at handling complex background changes. Our approach preserves the semantics of the original object (Figure 1) by conditioning the text-to-image diffusion model on object boundaries and textual descriptions generated by image-to-segment [31] and image-to-text [33] models. We guide the diffusion model by adding the desired textual description or optimizing its latent visual representation and textual embedding for generating diverse natural and adversarial background changes. Furthermore, we generate datasets covering diverse background changes on a selected subset of ImageNet [10] and COCO validation set [36] enabling comprehensive evaluation of modern uni-modal and multi-modal models across different tasks. Our contribution are as follows:

- We propose OBJECTCOMPOSE, an automated approach to introduce diverse background changes to real images, allowing us to evaluate resilience of modern vision-based models against object-to-background context.
- Our proposed background changes result in an average performance drop of 13.64% on classifier models compared to the baseline method, and a more substantial drop of 68.71% when exposed to adversarial background alterations (see Table 1).
- Object detection and segmentation models, which incorporate object-to-background context, display reasonably better robustness to background changes than classification models (see Table 5 and Figure 8).
- Models trained on large-scale datasets with scalable and stable training show better robustness against background changes (see Figure 7 and Table 2).

## 2 Related Work

**Common Corruptions.** In [66], different datasets are curated by separating foreground and background elements using ImageNet-1k bounding boxes.

They found that models could achieve high object classification performance even when the actual object was absent. Similarly, [48] demonstrate that subtle changes in object positioning could significantly impact the detector’s predictions, highlighting the sensitivity of these models to spatial configurations. A related approach by [53] focuses on co-occurring objects within an image and investigates if removing one object affected the response of the target model toward another. [60] analyze the models’ reliance on background signals for decision-making by training on various synthetic datasets. [21] benchmark the robustness of classifiers against common corruptions and perturbations like fog, blur, and contrast variations. In subsequent work, [22] introduce ImageNet-A dataset, filtering natural adversarial examples from a subset of ImageNet to limit spurious background cues. Also, [20] introduce the ImageNet-R dataset, which comprises various renditions of object classes under diverse visual representations such as paintings, cartoons, embroidery, sculptures, and origami. Similarly, [41] introduce the RIVAL10 dataset to study Gaussian noise corruptions in the foreground, background, and object attributes.

**Viewpoint Changes.** [1, 5, 15] introduce a large-scale 3D shape datasets to study object scale and viewpoints variations. In a similar vein, [28] introduce a synthetic dataset of rendered objects to aid in diagnostic evaluations of visual question-answering models. Later works have made strides in addressing the realism gap. [2] utilize crowd-sourcing to control rotation, viewpoints, and backgrounds of household objects, while [27] provide more fine-grained annotations for variations on the ImageNet validation set. In a recent development, [3] released PUG dataset rendered using Unreal Engine under diverse conditions, including varying sizes, backgrounds, camera orientations, and light intensities. While these methods offer control over changing several attributes in images, they lack in realism and are not suitable for our primary goal of studying object-to-background context in real images. In contrast, our proposed framework can generate a wide range of object-to-background compositional changes that can influence the models performance.

**Adversarial and Counterfactual Manipulations.** Researchers have uncovered that subtle, carefully designed alterations to an image, imperceptible to human observers, have the ability to deceive deep learning models [16, 32, 58]. These perturbations, constructed using gradient-based methods, serve as a worst-case analysis in probing the model’s robustness within specified distance norm metrics ( $l_2$  or  $l_\infty$ ). Another strategy entails applying unbounded perturbations to specific image patches, thereby conserving object semantics while inducing model confusion [12, 52]. Recent studies also leverage generative models to create semantic adversarial alterations in images [6, 7, 17, 26, 35, 45, 56]. In [45], LANCE framework is proposed which utilises fine-tuned large language models to get the modified textual prompt for editing of real images to evaluate model’s robustness. However, this framework is not suitable for studying object-to-background compositional changes since the prompt-to-prompt [23] based image editing method leads to global changes in the scene, often altering the object semantics. This necessitates hyper-parameter tuning of parameters

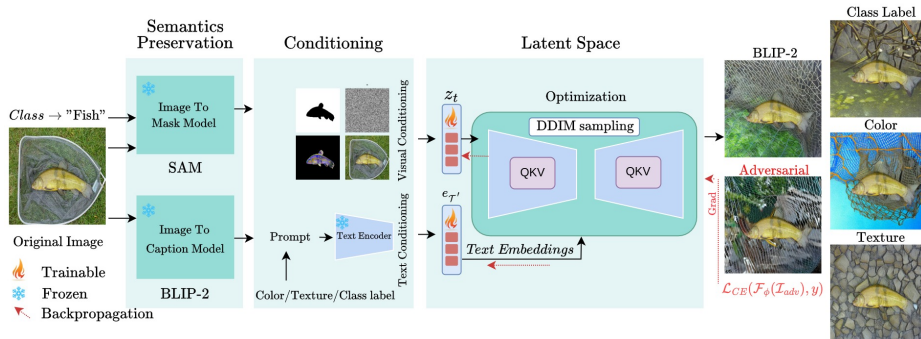


**Fig. 2:** OBJECTCOMPOSE consists of an inpainting-based diffusion model to generate the counterfactual background of an image. The object mask is obtained from a segmentation model (SAM) by providing the class label as an input prompt. The segmentation mask, along with the original image caption (generated via BLIP-2) is then processed through the diffusion model. For generating adversarial examples, both the latent and conditional embedding are optimized during the denoising process.

used for prompt-to-prompt editing, leading to generation of multiple edited image versions and selecting the one most faithful to the original image. In [35], using already available masks of ImageNet dataset [13], diffusion model is utilised to alter the background of images by varying its texture. A complexity loss based on gray-level co-occurrence matrix [18] of the image is used during the denoising process to vary the complexity of the background. On the contrary, our method can induce natural background variations through textual guidance and optimize the latent space of the diffusion model for adversarial changes.

### 3 Method

We introduce OBJECTCOMPOSE, our method for generating diverse language-guided object-to-background compositional changes to evaluate the resilience of current vision-based models. OBJECTCOMPOSE does this by exploiting the complementary strength of foundational models; image-to-segment, and image-to-text to guide object-preserving diffusion inference for natural and adversarial background-to-object context variations (see Figure 2). Our automated approach effectively generates different datasets under varying distribution shifts, which can be used for benchmarking vision and vision language models.

In Section 3.1, we provide the preliminaries of text-to-image, image-to-text, and image-to-segment models that are used in our method. Subsequently, in Section 3.2, we explain the working of our method in detail.

#### 3.1 Preliminaries

**Diffusion Models.** Diffusion models have made remarkable advancements in generating high quality images and refining them based on textual guidance.

During training, diverse noisy versions  $\mathcal{I}_t$  of the clean image  $\mathcal{I}$  are fed into the diffusion model  $\epsilon_\theta$  at different time steps  $t$ . The objective for the model is to learn the specific noise added at each time step. The training process of diffusion models comprises of two stages; in the forward process (*first stage*) gaussian noise sampled from a normal distribution  $\mathcal{N}(0, I)$  is gradually added to image  $\mathcal{I}$  according to a variance schedule ( $\beta_t : t = 1, \dots, T$ ). Using the reparameterization trick, we can get the noisy image  $\mathcal{I}_t$  at any time step as follows:

$$\mathcal{I}_t = \sqrt{\alpha_t}\mathcal{I} + \sqrt{1 - \alpha_t}\epsilon \quad \epsilon \sim \mathcal{N}(0, I) \quad (1)$$

Here,  $\alpha_t = 1 - \beta_t$  and  $\bar{\alpha}_t = \prod_{s=1}^t \alpha_s$ . As  $T \rightarrow \infty$ ,  $\bar{\alpha}_T \rightarrow 0$ , which implies  $\mathcal{I}_T \sim \mathcal{N}(0, I)$ , all the information of the original image  $\mathcal{I}$  will be lost. Typically, diffusion models are conditioned on the time step  $t$  and additional factors like the class label  $\mathbf{y}$  or textual description  $\mathcal{T}$ . However, recent works have extended this conditioning to also consider the clean image  $\mathcal{I}$  and its corresponding mask, enabling specialized image editing tasks [47, 49]. Next, in the reverse process (*second stage*) based on the conditioning, a model  $\epsilon_\theta$  is learned to approximate the gaussian parameters at each time step  $t$  for the true reverse conditional distribution. Essentially, the training objective  $l_t$  minimizes the error between the estimated and actual noise added to the image at different time steps  $t$ :

$$L_t = \|\epsilon - \epsilon_\theta^t(\mathcal{I}_t, e_{\mathcal{T}}, \psi)\|^2 \quad (2)$$

where  $e_{\mathcal{T}}$  is the embedding of conditional guidance through either class label or caption of the image and  $\psi$  is any additional conditioning, such as mask or layout of the scene.

**Foundational Models.** BLIP-2 [33] presents an efficient vision-language pre-training approach that utilizes a lightweight Querying Transformer (QFormer) to bridge the modality gap between pre-trained vision and large language models (LLMs). This framework initially passes the image through a pre-trained vision encoder and extracts relevant features via the QFormer. This information is then passed to the pre-trained LLM to obtain a descriptive caption of the image.

Recently, Segment Anything Model (SAM) [31], a image segmentation model was introduced, that undergoes pre-training on an extensive dataset of high quality images. SAM employs prompts, which can manifest in various forms such as point sets, boxes, masks, or textual input, to demarcate objects within an image. The image initially undergoes an encoding process through a large transformer-based image encoder. Subsequently, both the features extracted from the image and the embeddings of the prompt from a prompt encoder traverse a lightweight decoder, yielding the desired segmentation mask.

### 3.2 Object-to-Background Compositional Changes

In order to generate object-to-background compositional changes without altering object semantics our method consists of an Object-to-Background Conditioning module to provide strong visual guidance to the text-to-image diffusion model. In the next stage, we condition the diffusion model on the textual prompt

to introduce desired background changes or optimize the latent representation and textual embedding in order to generate adversarial backgrounds.

**Preserving Object Semantics.** We propose an Object-to-Background Conditioning Module denoted as  $\mathcal{C}$ , which takes the input image  $\mathcal{I}$  and the provided label  $\mathbf{y}$  as inputs, and returns both the textual prompt  $\mathcal{T}$  describing the scene and mask  $\mathcal{M}$  encapsulates the object in the image:

$$\mathcal{C}(\mathcal{I}, \mathbf{y}) = \mathcal{T}, \mathcal{M} \quad (3)$$

Our conditioning module leverages a promptable segmentation model called SAM [31] denoted by  $\mathcal{S}$ . By passing the class information  $\mathbf{y}$  and the image  $\mathcal{I}$  to the model  $\mathcal{S}(\mathcal{I}, \mathbf{y})$ , we obtain the object mask  $\mathcal{M}$ . Simultaneously, to acquire a description for the image scene, we utilize BLIP-2 [34], an image-to-text model denoted as  $\mathcal{B}$  to get the necessary prompt  $\mathcal{T}_{\mathcal{B}}$  describing the scene, thereby providing object-to-background context information.

$$\mathcal{B}(\mathcal{I}) = \mathcal{T}_{\mathcal{B}} \quad ; \quad \mathcal{S}(\mathcal{I}, \mathbf{y}) = \mathcal{M} \quad (4)$$

The mask  $\mathcal{M}$  and the textual prompt  $\mathcal{T}_{\mathcal{B}}$  serve as conditioning inputs for the subsequent stage, where we employ a diffusion model to generate diverse background variations. This methodical integration of segmentation and language comprehension offers fine-grained control over image backgrounds while upholding object semantics, leading to refined object-centric image manipulations. It’s worth noting that we have the flexibility to choose any desired textual prompt  $\mathcal{T}$ , and are not confined to using  $\mathcal{T}_{\mathcal{B}}$  as the textual condition.

**Background Generation.** Once we’ve obtained both visual and textual information  $(\mathcal{T}, \mathcal{M})$  from our conditioning module, we employ a diffusion model that has been trained for inpainting tasks, which has additional conditioning  $\psi$  comprising of the image  $\mathcal{I}$  and its corresponding mask  $\mathcal{M}$ . The denoising operation takes place in the latent space instead of the image pixel space, which is facilitated through the use of a variational autoencoder that provides the mapping between images and their respective latent representations. During the denoising stage, starting with a standard normal Gaussian noise latent  $z_t$ , the diffusion model calculates the estimated noise  $\hat{\epsilon}_{\theta}^t$  to be removed from the latent at time step  $t$  using a linear combination of the noise estimate conditioned on the textual description  $\epsilon_{\theta}^t(z_t, e_{\mathcal{T}}, i, m)$  and the unconditioned estimate  $\epsilon_{\theta}^t(z_t, i, m)$ :

$$\hat{\epsilon}_{\theta}^t(z_t, e_{\mathcal{T}}, i, m) = \epsilon_{\theta}^t(z_t, i, m) + \lambda (\epsilon_{\theta}^t(z_t, e_{\mathcal{T}}, i, m) - \epsilon_{\theta}^t(z_t, i, m)) \quad (5)$$

Here,  $(i, m)$  represents the representation of the original image  $\mathcal{I}$  and its corresponding mask  $\mathcal{M}$  in the latent space. The guidance scale  $\lambda$  determines how much the unconditional noise estimate  $\epsilon_{\theta}(z_t, i, m)$  should be adjusted in the direction of the conditional estimate  $\epsilon_{\theta}(z_t, e_{\mathcal{T}}, i, m)$  to closely align with the provided textual description  $\mathcal{T}$  (see Appendix A.1). In this whole denoising process, the mask  $\mathcal{M}$  generated from our conditioning module guides the image alterations to the background of the object, while the textual description  $\mathcal{T}$  contains information for the desired background change.

Our method also handles adversarial background changes by optimizing the conditioned visual and textual latents  $z_t$  and  $e_{\mathcal{T}}$  through a discriminative model  $\mathcal{F}_\phi$  to craft adversaries. For generating adversarial examples the goal of the attacker is to craft perturbations  $\delta$  that when added to clean image  $\mathcal{I}$  with class label  $\mathbf{y}$ , result in an adversarial image  $\mathcal{I}_{adv} = \mathcal{I} + \delta$  which elicits an incorrect response from a classifier model  $\mathcal{F}_\phi$  i.e.,  $\mathcal{F}_\phi(\mathcal{I}_{adv}) \neq \mathbf{y}$ , where  $\phi$  are the model parameters. Usually in pixel-based perturbations,  $\delta$  is bounded by a norm distance, such as  $l_2$  or  $l_\infty$  norm to put a constraint on pixel-level changes done to preserve the semantics of the image. However, in our setting, the control on the amount of perturbation added is governed by the textual and visual latent passed to the diffusion model. In our method (see Algo. 1), we use the discriminative model  $\mathcal{F}_\phi$  to guide the diffusion model  $\epsilon_\theta$  to generate adversarial examples by optimizing its latent representations  $z_t$  and  $e_{\mathcal{T}}$ :

$$\max_{z_t, e_{\mathcal{T}}} \mathcal{L}_{adv} = \mathcal{L}_{CE}(\mathcal{F}_\phi(\mathcal{I}_{adv}), \mathbf{y}) \quad (6)$$

where  $\mathcal{L}_{CE}$  is the cross-entropy loss,  $e_{\mathcal{T}}$  is textual embedding and  $z_t$  is the denoised latent at time step  $t$ .  $\mathcal{I}_{adv}$  represents the image generated by the diffusion model after it has been denoised using DDIM [55], a deterministic sampling process in which the latent update is formulated as:

$$z_{t-1} = \sqrt{\bar{\alpha}_{t-1}} \left( \frac{z_t - \sqrt{1 - \bar{\alpha}_t} \hat{\epsilon}_\theta^t}{\sqrt{\bar{\alpha}_t}} \right) + \sqrt{1 - \bar{\alpha}_{t-1}} \hat{\epsilon}_\theta^t, \quad t = T, \dots, t-1, \dots, 1 \quad (7)$$

Our proposed unconstrained adversarial objective  $\mathcal{L}_{adv}$  would lead to unrestricted changes in the image background while object semantics are preserved by using the mask conditioning from  $\mathcal{S}$ .

## 4 Experimental Protocols

**Dataset Preparation.** For classification, we initially gathered 30k images from the ImageNet validation set [10], which are correctly classified with high success rate using an ensemble of models; ViT-T, ViT-S [11], Res-50, Res-152 [19], Dense-161 [25], Swin-T, and Swin-S [37]. In order to create a high-quality dataset for our object-to-context variation task, we remove image samples where the boundary between foreground and background is not distinct, e.g., "mountain tent" where the mountain might appear in the background of the tent. This processing results in 15k images. Then for foreground semantic preservation, we utilize a compute-efficient variant of SAM, known as FastSAM [64] with class labels as prompts to generate segmentation masks of the foreground object. However, FastSAM encounter challenges in accurately segmenting objects in all images. To address this, we selected images where the mask-creation process demonstrated exceptional accuracy and generated a clear separation between the object of interest and its background. This meticulous selection process yield a curated dataset comprising 5,505 images, representing a subset of 582 ImageNet classes.



We refer to this dataset as **ImageNet-B**. More details are presented in Appendix A.17. Due to the computational cost involved in adversarial background optimization and running baseline methods, we select a subset of 1000 images from 500 classes of **ImageNet-B** by sampling two images from each class for comparison. We refer to this dataset as **ImageNet-B<sub>1000</sub>**. Rest of our experiments are performed on the full **ImageNet-B** dataset.

For object detection, we carefully filtered 1,127 images manually from the COCO 2017 validation set [36], with a clear distinction between foreground objects and their background. We refer to these images as **COCO-DC**. We use **COCO-DC** to evaluate both detection and classification. The dataset can have multiple objects in the image. To use this dataset for classification we train the above-mentioned models on the COCO train dataset using labels associated with the object that occupies the highest mask region in the image and evaluated on our generated dataset.

**Diffusion Parameters.** We use the pre-trained Inpaint Stable Diffusion v2 [47] as our text-to-image model and set the guidance parameter  $\lambda$  to 7.5, and use the DDIM sampling [55] with  $T = 20$  timesteps. We craft adversarial examples on **ImageNet-B<sub>1000</sub>** using Res-50 [19] as the classifier model and maximize the adversarial loss  $\mathcal{L}_{adv}$  shown in Eq.6 for 30 iterations. For **COCO-DC**, we maximize the loss in the feature space of the model. Both the text embedding  $e_{\mathcal{T}}$  of the prompt  $\mathcal{T}$  (initialized with  $\mathcal{T}_B$ ) and denoised latent  $z_t$  are optimized from denoising time step  $t = 4$  using AdamW [39] with a learning rate of 0.1. All experiments were conducted using a single NVIDIA-A100 GPU.

**Vision Models.** We conducted evaluations for the classification task using a diverse set of models. *a) Natural ImageNet Training:* We evaluate seven naturally ImageNet-trained vision transformers and convolutional neural networks (CNNs). Specifically we use ViT-T, ViT-S [11], Res-50, Res-152 [19], Dense-161 [25], Swin-T, and Swin-S [37]. *b) Adversarial ImageNet Training:* We also evaluate adversarial ImageNet-trained models including ResAdv-18, ResAdv-50, and WideResAdv-50 at various perturbation budget of  $\ell_\infty$  and  $\ell_2$  [50]. *c) Multimodal Training:* Additionally, we explored seven vision language foundational models within CLIP [46] and EVA-CLIP [57]. *d) Stylized ImageNet Training:* We evaluate the DeiT-T and DeiT-S models trained on a stylized version of the ImageNet dataset [14,43]. *e) Self-Supervised Training:* We evaluate the performance of DINOv2 models with registers [9,44] which are trained in a self-supervised manner on a large-scale curated dataset LVD-142M, and subsequently fine-tuned on ImageNet. *f) Segmentation and Detection:* We evaluate Mask-RCNN for segmentation and object detection respectively using our proposed background-to-object variations. Evaluations on FastSAM [64] and DETR [4] are reported in Appendix A.11 and A.10. *g) Image Captioning:* We also evaluate the robustness of a recent image captioning model BLIP-2 [34], using our generated dataset. For the task *a)*, and *b)*, we provide comparison with the baseline methods on **ImageNet-B<sub>1000</sub>** and report results on **ImageNet-B** in the Appendix A.5.

**Evaluation Metrics:** We report results using the top-1 accuracy (%), Intersection Over Union (IoU), Average Precision(AP) and Recall(AR), and CLIP text

**Table 1:** Resilience evaluation of vision models on ImageNet-B<sub>1000</sub> (Top-1 (%) accuracy). Our natural object-to-background changes, including color and texture, perform favorably against state-of-the-art methods. Furthermore, our adversarial object-to-background changes show a significant drop in performance across vision models.

Datasets	ViT				CNN			Average
	ViT-T	ViT-S	Swin-T	Swin-S	Res-50	Res-152	Dense-161	
Original	95.5	97.5	97.9	98.3	98.5	99.1	97.2	97.71
ImageNet-E ( $\lambda=-20$ )	91.3	94.5	96.5	97.7	96.0	97.6	95.4	95.50 (-2.21)
ImageNet-E ( $\lambda=20$ )	90.4	94.5	95.9	97.4	95.4	97.4	95.0	95.19 (-2.52)
ImageNet-E ( $\lambda_{adv} = 20$ )	82.8	88.8	90.7	92.8	91.6	94.2	90.4	90.21 (-7.50)
LANCE	80.0	83.8	87.6	87.7	86.1	87.4	85.1	85.38 (-12.33)
Class label	90.5	94.0	95.1	95.4	96.7	96.5	94.7	94.70 (-3.01)
BLIP-2 Caption	85.5	89.1	91.9	92.1	93.9	94.5	90.6	91.08 (-6.63)
Color	67.1	83.8	85.8	86.1	88.2	91.7	80.9	83.37 (-14.34)
Texture	64.7	80.4	84.1	85.8	85.5	90.1	80.3	81.55 (-16.16)
Adversarial	18.4	32.1	25.0	31.7	2.0	14.0	28.0	21.65 (-76.06)

similarity score for classification, segmentation, object detection, and captioning tasks, respectively.

**Background Conditioning.** During inducing background variations, we use the following text prompts templates; Class Label: "*A picture of a class*" where *class* is the class name of the image, Caption: "*captions from BLIP-2 model*", Color: "*A picture of \_\_\_ background*" where *\_\_\_* is replaced with red, green, blue, and colorful, Texture: "*A picture of \_\_\_ background*" where *\_\_\_* is replaced with textured, intricately rich textures, colorful textures, distorted textures, Adversarial: "*captions from BLIP-2 model*". Note that for adversarial setting the text prompts get updated after optimization. In the case of the ImageNet-E method [35], default values of  $\lambda$  are employed to regulate the strength of texture complexity introduced in both natural and adversarial background changes. Likewise, for LANCE [45], the default prompt specified in the paper is utilized, passing it to the large language model to generate variations of captions that reflect background changes. We observe similar trends across different color and texture prompts and report the worst-performing one. Detailed analysis across different color and texture prompts is provided in Appendix A.5.

#### 4.1 Comparison with Baseline Methods

**Natural ImageNet Training.** In Table 1, we observe that background variations introduced by our method are more challenging for vision models, resulting in a performance drop of 13.5% compared to ImageNet-E ( $\lambda = 20$ ) on natural background variations. When subjected to adversarial background changes, a substantial performance drop of 68.56% is observed compared to ImageNet-E ( $\lambda_{adv} = 20$ ), highlighting the effectiveness of the unconstrained nature of our attack. Background variations by our method show a consistent decline in accuracy for both transformer-based and CNN models when exposed to diverse

**Table 2:** Resilience evaluation of Zero-shot CLIP and EVA-CLIP models on **ImageNet-B<sub>1000</sub>** (Top-1 (%) accuracy). Our natural object-to-background changes, including color and texture, perform favorably against state-of-the-art methods. We find that EVA-CLIP models show better performance across all background variations.

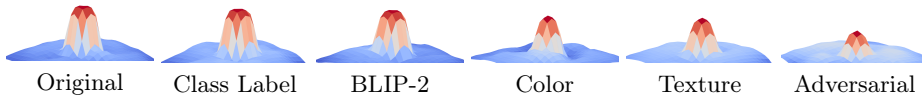
Datasets	CLIP							Average
	ViT-B/32	ViT-B/16	ViT-L/14	Res50	Res101	Res50x4	Res50x16	
Original	73.90	79.40	87.79	70.69	71.80	76.29	82.19	77.43
ImageNet-E ( $\lambda=20$ )	69.79	76.70	82.89	67.80	69.99	72.70	77.00	73.83 <sub>(-3.60)</sub>
ImageNet-E ( $\lambda=20$ )	67.97	76.16	82.12	67.37	39.89	72.62	77.07	73.31 <sub>(-4.12)</sub>
ImageNet-E ( $\lambda_{adv} = 20$ )	62.82	70.50	77.57	59.98	65.85	67.07	67.07	68.23 <sub>(-9.20)</sub>
LANCE	54.99	54.19	57.48	58.05	60.02	60.39	73.37	59.78 <sub>(-17.65)</sub>
Class label	78.49	83.66	81.58	76.60	77.00	82.09	84.50	80.55 <sub>(+3.12)</sub>
BLIP-2 Captions	68.79	72.29	71.49	65.20	68.40	71.20	75.40	70.40 <sub>(-7.03)</sub>
Color	48.30	61.00	69.51	50.50	54.80	60.30	69.28	59.14 <sub>(-18.29)</sub>
Texture	49.60	62.41	58.88	51.69	53.20	60.79	67.49	57.71 <sub>(-19.72)</sub>
Adversarial	25.5	34.89	48.19	18.29	24.40	30.29	48.49	32.87 <sub>(-46.25)</sub>

Datasets	EVA-CLIP							Average
	g/14	g/14+	B/16	L/14	L/14+	E/14	E/14+	
Original	88.80	92.69	89.19	91.10	91.99	93.80	94.60	91.74
ImageNet-E ( $\lambda=20$ )	84.74	88.98	85.55	89.19	88.78	92.02	91.81	88.72 <sub>(-3.02)</sub>
ImageNet-E ( $\lambda=20$ )	84.10	89.40	85.81	88.51	89.69	92.69	92.50	88.95 <sub>(-2.79)</sub>
ImageNet-E ( $\lambda_{adv} = 20$ )	79.69	85.45	80.20	84.04	85.95	89.89	89.59	84.97 <sub>(-6.77)</sub>
LANCE	70.25	77.40	73.26	76.63	77.46	80.95	78.65	76.37 <sub>(-15.37)</sub>
Class label	90.10	92.90	88.61	91.31	91.90	93.40	93.41	91.66 <sub>(-0.08)</sub>
BLIP-2 Caption	80.31	84.29	82.10	82.50	84.80	86.90	86.90	83.97 <sub>(-7.77)</sub>
Color	73.50	80.50	73.20	80.70	84.61	84.39	87.00	80.55 <sub>(-11.19)</sub>
Texture	75.30	78.90	74.40	80.80	82.10	83.60	85.60	80.10 <sub>(-11.64)</sub>
Adversarial	55.59	62.49	48.70	65.39	73.59	70.29	73.29	64.19 <sub>(-27.55)</sub>

object-to-background changes. This decrease is especially noticeable in texture and color backgrounds. We find that as we moved from purely transformer-based architectures to convolution-based architectures, there is an overall improvement in accuracy across natural background changes. For instance, the average accuracy across all backgrounds for ViT-T, Swin-T, and Res-50 on **ImageNet-B<sub>1000</sub>** is 76.95%, 89.22% and 91.08% respectively. Further, we observe that as the model capacity is increased across different model families, the robustness to background changes also increases. As is evident, the models are most vulnerable to adversarial background changes, resulting in a significant drop in average accuracy. Res-50 shows most drop on adversarial changes, which is expected as it serves as the discriminative model  $\mathcal{F}_\phi$  (Eq. 6) for generating adversarial examples. In Figure 3, we depict the loss surfaces of ViT-S and observe that these surfaces become narrower and shallower with more pronounced background variations, aligning with our results. We provide results on **ImageNet-B** and **COCO-DC** dataset in Appendix A.5 and A.7 with ablations across different background prompts. Visualizations are provided in Figure 4 and Appendix A.13.

**Multimodal Training.** In Table 2, we observe that compared to ImageNet-E ( $\lambda = 20$ ), our natural background variations lead to an average performance drop of 15.66% and 8.85% on CLIP and EVA-CLIP models. On comparing with ImageNet-E ( $\lambda_{adv} = 20$ ), our adversarial background variations lead to an av-



**Fig. 3:** The loss surfaces (*flipped*) of the ViT-S depicted on **ImageNet-B**. Significant distribution shifts result in narrow and shallow surfaces at convergence.

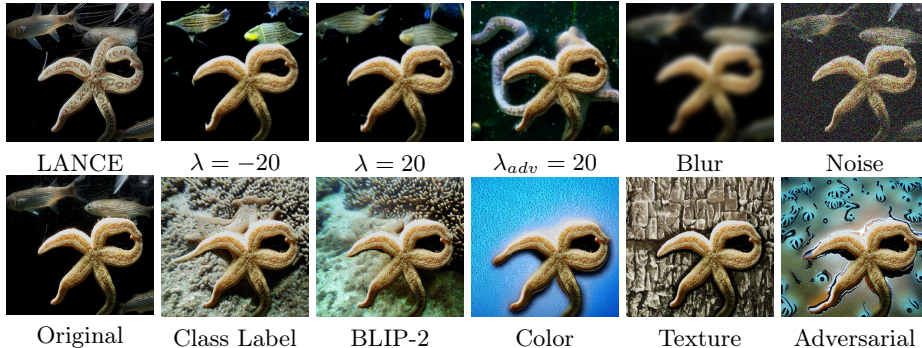


**Fig. 4:** Qualitative comparison of our method (*bottom row*) with previous related work (*top row*). Our method enables diversity and controlled background edits.

erage performance drop of 35.36% and 20.78% on CLIP and EVA-CLIP models. Similar to results mentioned in Table 1, zero-shot robustness shows similar trend across different background changes. However, for background variations induced using class label information the performance increases in CLIP-based models. This reason could be the use of CLIP text encoder utilized for generating the textual embedding  $e_{\mathcal{T}}$  for guiding the generation process of the diffusion model. On EVA-CLIP, which proposed changes to stabilize the training of CLIP models on large-scale datasets, we observe significant improvement in zero-shot performance across all background changes. In Appendix A.5, we delve into the comparison between multimodal and unimodal models, offering detailed results on **ImageNet-B** dataset.

**Object Semantic distortion:** It’s noteworthy to mention that in both Table 1 and 2, we observe a significant drop in performance of models across background changes induced by LANCE method. However, we discover that the drop in performance is not necessarily due to the induced background changes, rather than distorting the object semantics, making it unsuitable for evaluating object-to-background context. This observation is supported by Figure 5, where we evaluate performance on original and LANCE generate images while masking the background. A significant performance drop is evident across all models, emphasizing the distortion of object semantics. For a more detailed discussion and visualizations, please refer to Appendix A.3 and A.4.

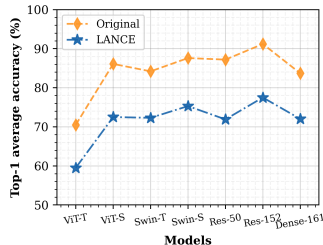


**Fig. 5:** Evaluating LANCE on **ImageNet-B**<sub>1000</sub> dataset with masked background.

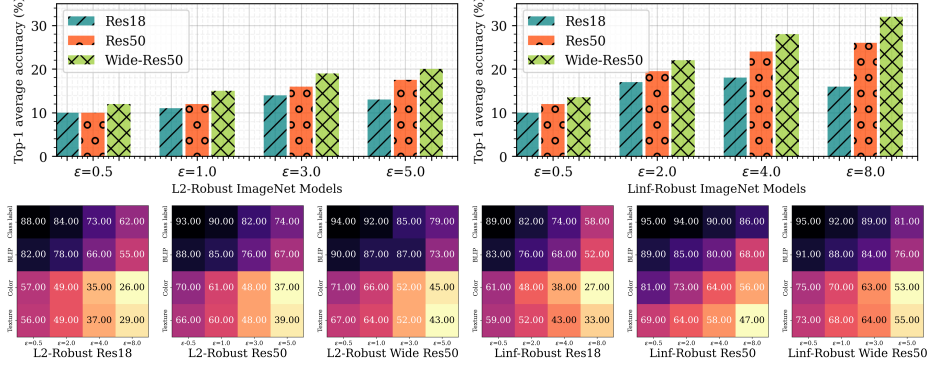


**Fig. 6:** Evaluating Adversarially trained models: The top row plots the Top-1(%) accuracy achieved by adversarially trained ResNet models on adversarial background changes on **ImageNet-B<sub>1000</sub>** and the bottom row indicates for the case of non-adversarial background changes on **ImageNet-B**.

## 4.2 Further Evaluations

**Adversarial ImageNet Training.** As can be seen from Figure 6 (*bottom row*), our object-to-background compositional changes on **ImageNet-B** lead to a significant decline in accuracy for adversarially trained models. This highlights the robustness of these models is limited to adversarial perturbations and does not transfer to different distribution shifts. In Figure 6 (*top row*), when we evaluate these models on adversarial background changes on **ImageNet-B<sub>1000</sub>**, the performance improves with an increase in adversarial robustness( $\epsilon$ ) of the models. Furthermore, we also observe models with more capacity perform better, similar to results on natural training. For detailed results and comparison with baseline methods, refer to Appendix A.6.

**Stylized ImageNet Training.** Despite the focus of Stylized ImageNet training [14] to encourage models to concentrate on the foreground of the scene by reducing background cues for prediction [43], our findings indicate that it is still susceptible to both natural and adversarial object-to-background variations (see Table 3). Consequently, its applicability appears to be constrained to specific distribution shifts.

**Self-Supervised Training.** Improved performance is observed in Dinov2 models across object-to-background variations (see Figure 7). We hypothesize this improvement is acquired through training on extensive curated datasets and the utilization of additional learnable registers/tokens during training for refining the interpretability of attention maps. For more details, refer to Appendix A.8.

**Segmentation and Detection.** We observe a consistent decrease in AP scores on the task of object detection and instance segmentation across different back-

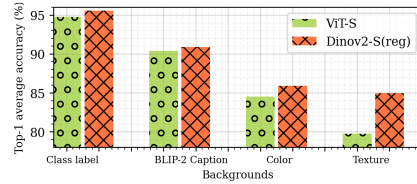


**Fig. 7:** Evaluating Dinov2 models on **ImageNet-B** background changes.

**Table 3:** Stylized Training Evaluation

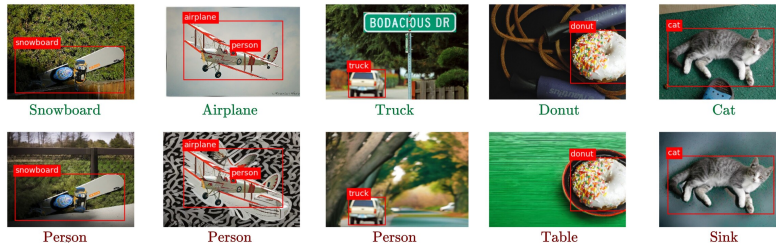
Datasets	Background	Stylized Trained models		
		DeiT-S	DeiT-T	Average
ImageNet-B	Original	91.22	87.21	89.21
	Class label	89.35	85.35	87.35 (-1.86)
	BLIP-2 Caption	84.01	79.19	81.60 (-7.61)
	Color	66.57	57.54	62.05 (-27.13)
ImageNet-B <sub>1000</sub>	Texture	64.08	54.82	59.45 (-29.76)
	Adversarial	15.90	10.80	13.35 (-74.40)

**Table 4:** Image-to-Caption (BLIP-2) Evaluation

Dataset	Background	CLIP Score
ImageNet-B	Class Label	0.75
	BLIP-2 Caption	0.84
	Color	0.66
	Texture	0.67
ImageNet-B <sub>1000</sub>	Adversarial	0.62

**Table 5:** Mask AP and Segment AP score on COCO-DC

Background	Box AP	Segment AP
Original	57.99	56.29
BLIP-2 Caption	47.40	44.75
Color	48.12	45.09
Texture	45.79	43.07
Adversarial	37.10	34.91

**Fig. 8:** Correct predictions by Mask-RCNN and Res-50 on the original image (*top row*) and the corresponding predictions on altered backgrounds (*bottom row*).

ground variations generated on COCO-DC(see Table 5). The adversarial background results in the lowest AP scores, but still remains at a reasonable level given that the adversarial examples are generated using a classification model, with limited cross-task transferability. Moreover, our qualitative observations suggest detection and segmentation models exhibit greater resilience to changes in the background compared to classifiers (see Figure 8 and Appendix A.10).

**Image Captioning.** Table 4 reports the CLIP score between the captions obtained on the clean and generated images using BLIP-2 model. The scores decrease across color, texture, and adversarial background changes. For qualitative results, see Appendix A.9.

## 5 Conclusion

In this study, we propose OBJECTCOMPOSE, a method for generating object-to-background compositional changes. Our method addresses the limitations of current works, specifically distortion of object semantics and diversity in background changes. We accomplish this by utilizing the capabilities of image-to-text and image-to-segmentation foundational models to preserve the object semantics, while we optimize for diverse object-to-background compositional changes by modifying the textual prompts or optimizing the latents of the text-to-image model. OBJECTCOMPOSE offers a complimentary evaluation protocol to the existing ones, for comprehensive evaluations across current vision-based models to reveal their vulnerability to background alterations. We anticipate that our insights will pave the way for a more thorough evaluation of vision models, consequently driving the development of more effective methods for improving their resilience.



## References

1. Alcorn, M.A., Li, Q., Gong, Z., Wang, C., Mai, L., Ku, W.S., Nguyen, A.: Strike (with) a pose: Neural networks are easily fooled by strange poses of familiar objects. In: *Proceedings of the IEEE/CVF conference on computer vision and pattern recognition*. pp. 4845–4854 (2019)
2. Barbu, A., Mayo, D., Alverio, J., Luo, W., Wang, C., Gutfreund, D., Tenenbaum, J., Katz, B.: Objectnet: A large-scale bias-controlled dataset for pushing the limits of object recognition models. *Advances in neural information processing systems* **32** (2019)
3. Bordes, F., Shekhar, S., Ibrahim, M., Bouchacourt, D., Vincent, P., Morcos, A.S.: Pug: Photorealistic and semantically controllable synthetic data for representation learning (2023)
4. Carion, N., Massa, F., Synnaeve, G., Usunier, N., Kirillov, A., Zagoruyko, S.: End-to-end object detection with transformers. In: *European conference on computer vision*. pp. 213–229. Springer (2020)
5. Chang, A.X., Funkhouser, T., Guibas, L., Hanrahan, P., Huang, Q., Li, Z., Savarese, S., Savva, M., Song, S., Su, H., et al.: Shapenet: An information-rich 3d model repository. *arXiv preprint arXiv:1512.03012* (2015)
6. Chen, J., Chen, H., Chen, K., Zhang, Y., Zou, Z., Shi, Z.: Diffusion models for imperceptible and transferable adversarial attack (2023)
7. Christensen, P.E., Snæbjarnarson, V., Dittadi, A., Belongie, S., Benaim, S.: Assessing neural network robustness via adversarial pivotal tuning. *arXiv preprint arXiv:2211.09782* (2022)
8. Cubuk, E.D., Zoph, B., Mane, D., Vasudevan, V., Le, Q.V.: Autoaugment: Learning augmentation policies from data. *arXiv preprint arXiv:1805.09501* (2018)
9. Darcet, T., Oquab, M., Mairal, J., Bojanowski, P.: Vision transformers need registers. *arXiv preprint arXiv:2309.16588* (2023)
10. Deng, J., Dong, W., Socher, R., Li, L.J., Li, K., Fei-Fei, L.: Imagenet: A large-scale hierarchical image database. In: *2009 IEEE conference on computer vision and pattern recognition*. pp. 248–255. Ieee (2009)
11. Dosovitskiy, A., Beyer, L., Kolesnikov, A., Weissenborn, D., Zhai, X., Unterthiner, T., Dehghani, M., Minderer, M., Heigold, G., Gelly, S., et al.: An image is worth 16x16 words: Transformers for image recognition at scale. *arXiv preprint arXiv:2010.11929* (2020)
12. Fu, Y., Zhang, S., Wu, S., Wan, C., Lin, Y.: Patch-fool: Are vision transformers always robust against adversarial perturbations? *arXiv preprint arXiv:2203.08392* (2022)
13. Gao, S., Li, Z.Y., Yang, M.H., Cheng, M.M., Han, J., Torr, P.: Large-scale unsupervised semantic segmentation. *IEEE transactions on pattern analysis and machine intelligence* (2022)
14. Geirhos, R., Rubisch, P., Michaelis, C., Bethge, M., Wichmann, F.A., Brendel, W.: Imagenet-trained cnns are biased towards texture; increasing shape bias improves accuracy and robustness. *arXiv preprint arXiv:1811.12231* (2018)
15. Gondal, M.W., Wuthrich, M., Miladinovic, D., Locatello, F., Breidt, M., Volchkov, V., Akpo, J., Bachem, O., Schölkopf, B., Bauer, S.: On the transfer of inductive bias from simulation to the real world: a new disentanglement dataset. *Advances in Neural Information Processing Systems* **32** (2019)
16. Goodfellow, I.J., Shlens, J., Szegedy, C.: Explaining and harnessing adversarial examples. *arXiv preprint arXiv:1412.6572* (2014)

17. Goyal, S., Qin, C., Huang, P.S., Cengil, T., Dvijotham, K., Mann, T., Kohli, P.: Achieving robustness in the wild via adversarial mixing with disentangled representations. In: *Proceedings of the IEEE/CVF Conference on Computer Vision and Pattern Recognition*. pp. 1211–1220 (2020)
18. Haralick, R.M., Shanmugam, K., Dinstein, I.H.: Textural features for image classification. *IEEE Transactions on systems, man, and cybernetics* (6), 610–621 (1973)
19. He, K., Zhang, X., Ren, S., Sun, J.: Deep residual learning for image recognition. In: *Proceedings of the IEEE conference on computer vision and pattern recognition*. pp. 770–778 (2016)
20. Hendrycks, D., Basart, S., Mu, N., Kadavath, S., Wang, F., Dorundo, E., Desai, R., Zhu, T., Parajuli, S., Guo, M., et al.: The many faces of robustness: A critical analysis of out-of-distribution generalization. In: *Proceedings of the IEEE/CVF International Conference on Computer Vision*. pp. 8340–8349 (2021)
21. Hendrycks, D., Dietterich, T.: Benchmarking neural network robustness to common corruptions and perturbations. *arXiv preprint arXiv:1903.12261* (2019)
22. Hendrycks, D., Zhao, K., Basart, S., Steinhardt, J., Song, D.: Natural adversarial examples. In: *Proceedings of the IEEE/CVF Conference on Computer Vision and Pattern Recognition*. pp. 15262–15271 (2021)
23. Hertz, A., Mokady, R., Tenenbaum, J., Aberman, K., Pritch, Y., Cohen-Or, D.: Prompt-to-prompt image editing with cross attention control. *arXiv preprint arXiv:2208.01626* (2022)
24. Ho, J., Jain, A., Abbeel, P.: Denoising diffusion probabilistic models. *Advances in neural information processing systems* **33**, 6840–6851 (2020)
25. Huang, G., Liu, Z., Van Der Maaten, L., Weinberger, K.Q.: Densely connected convolutional networks. In: *Proceedings of the IEEE conference on computer vision and pattern recognition*. pp. 4700–4708 (2017)
26. Ibrahim, M., Garrido, Q., Morcos, A., Bouchacourt, D.: The robustness limits of sota vision models to natural variation. *arXiv preprint arXiv:2210.13604* (2022)
27. Idrissi, B.Y., Bouchacourt, D., Balestriero, R., Evtimov, I., Hazirbas, C., Ballas, N., Vincent, P., Drozdal, M., Lopez-Paz, D., Ibrahim, M.: Imagenet-x: Understanding model mistakes with factor of variation annotations. *arXiv preprint arXiv:2211.01866* (2022)
28. Johnson, J., Hariharan, B., Van Der Maaten, L., Fei-Fei, L., Lawrence Zitnick, C., Girshick, R.: Clevr: A diagnostic dataset for compositional language and elementary visual reasoning. In: *Proceedings of the IEEE conference on computer vision and pattern recognition*. pp. 2901–2910 (2017)
29. Kavar, B., Zada, S., Lang, O., Tov, O., Chang, H., Dekel, T., Mosseri, I., Irani, M.: Imagic: Text-based real image editing with diffusion models. In: *Proceedings of the IEEE/CVF Conference on Computer Vision and Pattern Recognition*. pp. 6007–6017 (2023)
30. Khattak, M.U., Rasheed, H., Maaz, M., Khan, S., Khan, F.S.: Maple: Multi-modal prompt learning. In: *Proceedings of the IEEE/CVF Conference on Computer Vision and Pattern Recognition*. pp. 19113–19122 (2023)
31. Kirillov, A., Mintun, E., Ravi, N., Mao, H., Rolland, C., Gustafson, L., Xiao, T., Whitehead, S., Berg, A.C., Lo, W.Y., et al.: Segment anything. *arXiv preprint arXiv:2304.02643* (2023)
32. Kurakin, A., Goodfellow, I., Bengio, S.: Adversarial machine learning at scale. *arXiv preprint arXiv:1611.01236* (2016)
33. Li, J., Li, D., Savarese, S., Hoi, S.: Blip-2: Bootstrapping language-image pre-training with frozen image encoders and large language models. *arXiv preprint arXiv:2301.12597* (2023)

34. Li, J., Li, D., Savarese, S., Hoi, S.: Blip-2: Bootstrapping language-image pre-training with frozen image encoders and large language models (2023)
35. Li, X., Chen, Y., Zhu, Y., Wang, S., Zhang, R., Xue, H.: Imagenet-e: Benchmarking neural network robustness via attribute editing. In: *Proceedings of the IEEE/CVF Conference on Computer Vision and Pattern Recognition*. pp. 20371–20381 (2023)
36. Lin, T.Y., Maire, M., Belongie, S., Bourdev, L., Girshick, R., Hays, J., Perona, P., Ramanan, D., Zitnick, C.L., Dollár, P.: Microsoft coco: Common objects in context (2015)
37. Liu, Z., Lin, Y., Cao, Y., Hu, H., Wei, Y., Zhang, Z., Lin, S., Guo, B.: Swin transformer: Hierarchical vision transformer using shifted windows (2021)
38. Liu, Z., Mao, H., Wu, C.Y., Feichtenhofer, C., Darrell, T., Xie, S.: A convnet for the 2020s. In: *Proceedings of the IEEE/CVF conference on computer vision and pattern recognition*. pp. 11976–11986 (2022)
39. Loshchilov, I., Hutter, F.: Decoupled weight decay regularization. *arXiv preprint arXiv:1711.05101* (2017)
40. Madry, A., Makelov, A., Schmidt, L., Tsipras, D., Vladu, A.: Towards deep learning models resistant to adversarial attacks. *arXiv preprint arXiv:1706.06083* (2017)
41. Moayeri, M., Pope, P., Balaji, Y., Feizi, S.: A comprehensive study of image classification model sensitivity to foregrounds, backgrounds, and visual attributes (2022)
42. Mokady, R., Hertz, A., Aberman, K., Pritch, Y., Cohen-Or, D.: Null-text inversion for editing real images using guided diffusion models. In: *Proceedings of the IEEE/CVF Conference on Computer Vision and Pattern Recognition*. pp. 6038–6047 (2023)
43. Naseer, M., Ranasinghe, K., Khan, S., Hayat, M., Khan, F.S., Yang, M.H.: Intriguing properties of vision transformers (2021)
44. Oquab, M., Darcet, T., Moutakanni, T., Vo, H., Szafraniec, M., Khalidov, V., Fernandez, P., Haziza, D., Massa, F., El-Nouby, A., et al.: Dinov2: Learning robust visual features without supervision. *arXiv preprint arXiv:2304.07193* (2023)
45. Prabhu, V., Yenamandra, S., Chattopadhyay, P., Hoffman, J.: Lance: Stress-testing visual models by generating language-guided counterfactual images (2023)
46. Radford, A., Kim, J.W., Hallacy, C., Ramesh, A., Goh, G., Agarwal, S., Sastry, G., Askell, A., Mishkin, P., Clark, J., Krueger, G., Sutskever, I.: Learning transferable visual models from natural language supervision (2021)
47. Rombach, R., Blattmann, A., Lorenz, D., Esser, P., Ommer, B.: High-resolution image synthesis with latent diffusion models. In: *Proceedings of the IEEE/CVF conference on computer vision and pattern recognition*. pp. 10684–10695 (2022)
48. Rosenfeld, A., Zemel, R., Tsotsos, J.K.: The elephant in the room. *arXiv preprint arXiv:1808.03305* (2018)
49. Saharia, C., Chan, W., Chang, H., Lee, C., Ho, J., Salimans, T., Fleet, D., Norouzi, M.: Palette: Image-to-image diffusion models. In: *ACM SIGGRAPH 2022 Conference Proceedings*. pp. 1–10 (2022)
50. Salman, H., Ilyas, A., Engstrom, L., Kapoor, A., Madry, A.: Do adversarially robust imagenet models transfer better? (2020)
51. Selvaraju, R.R., Cogswell, M., Das, A., Vedantam, R., Parikh, D., Batra, D.: Grad-CAM: Visual explanations from deep networks via gradient-based localization. *International Journal of Computer Vision* **128**(2), 336–359 (oct 2019). <https://doi.org/10.1007/s11263-019-01228-7>, <https://doi.org/10.1007/2Fs11263-019-01228-7>
52. Sharma, A., Bian, Y., Munz, P., Narayan, A.: Adversarial patch attacks and defences in vision-based tasks: A survey. *arXiv preprint arXiv:2206.08304* (2022)

53. Shetty, R., Schiele, B., Fritz, M.: Not using the car to see the sidewalk—quantifying and controlling the effects of context in classification and segmentation. In: Proceedings of the IEEE/CVF Conference on Computer Vision and Pattern Recognition. pp. 8218–8226 (2019)
54. Sitawarin, C., Pongmala, K., Chen, Y., Carlini, N., Wagner, D.: Part-based models improve adversarial robustness. arXiv preprint arXiv:2209.09117 (2022)
55. Song, J., Meng, C., Ermon, S.: Denoising diffusion implicit models. arXiv preprint arXiv:2010.02502 (2020)
56. Song, Y., Shu, R., Kushman, N., Ermon, S.: Constructing unrestricted adversarial examples with generative models. *Advances in Neural Information Processing Systems* **31** (2018)
57. Sun, Q., Fang, Y., Wu, L., Wang, X., Cao, Y.: Eva-clip: Improved training techniques for clip at scale. arXiv preprint arXiv:2303.15389 (2023)
58. Szegedy, C., Zaremba, W., Sutskever, I., Bruna, J., Erhan, D., Goodfellow, I., Fergus, R.: Intriguing properties of neural networks. arXiv preprint arXiv:1312.6199 (2013)
59. Touvron, H., Cord, M., Douze, M., Massa, F., Sablayrolles, A., Jégou, H.: Training data-efficient image transformers & distillation through attention. In: International conference on machine learning. pp. 10347–10357. PMLR (2021)
60. Xiao, K., Engstrom, L., Ilyas, A., Madry, A.: Noise or signal: The role of image backgrounds in object recognition (2020)
61. Yuan, Z., Cao, M., Wang, X., Qi, Z., Yuan, C., Shan, Y.: Customnet: Zero-shot object customization with variable-viewpoints in text-to-image diffusion models. arXiv preprint arXiv:2310.19784 (2023)
62. Yun, S., Han, D., Oh, S.J., Chun, S., Choe, J., Yoo, Y.: Cutmix: Regularization strategy to train strong classifiers with localizable features. In: Proceedings of the IEEE/CVF international conference on computer vision. pp. 6023–6032 (2019)
63. Zhang, H., Cisse, M., Dauphin, Y.N., Lopez-Paz, D.: mixup: Beyond empirical risk minimization. arXiv preprint arXiv:1710.09412 (2017)
64. Zhao, X., Ding, W., An, Y., Du, Y., Yu, T., Li, M., Tang, M., Wang, J.: Fast segment anything (2023)
65. Zhou, K., Yang, J., Loy, C.C., Liu, Z.: Learning to prompt for vision-language models. *International Journal of Computer Vision* **130**(9), 2337–2348 (2022)
66. Zhu, Z., Xie, L., Yuille, A.L.: Object recognition with and without objects. arXiv preprint arXiv:1611.06596 (2016)

## A Appendix

### Overview

- A.1. List of Prompts
- A.2. Algorithm
- A.3. Object Distortion in LANCE
- A.4. Qualitative Comparison with Related Works
- A.5. Ablation on Background Changes
- A.6. Evaluation on Adversarially Trained models
- A.7. Evaluation on Recent Vision models
- A.8. Evaluation on DINOv2 models
- A.9. Vision Language model for Image Captioning
- A.10. Qualitative Results on Detection
- A.11. Effect of Background Change on Segmentation Models
- A.12. Exploring Feature Space of Vision Models
- A.13. Diversity and Diffusion Parameter Ablation
- A.14. Misclassified Samples
- A.15. Limitations and Future Directions
- A.16. Potential External Factors
- A.17. Dataset Distribution
- A.18. Evaluation on Background/Foreground Images

#### A.1 List of prompts

We provide the list of prompts that are used to guide the diffusion model to generate diverse background changes, encompassing different distribution shifts with respect to the original data distribution.

**Table 6:** Prompts used to create background alterations

Background	Prompts
Class label	<i>"This is a picture of a class name"</i>
BLIP-2 Caption	Captions generated from BLIP-2 image to caption
Color <sub>prompt-1</sub>	<i>"This is a picture of a vivid red background"</i>
Color <sub>prompt-2</sub>	<i>"This is a picture of a vivid green background"</i>
Color <sub>prompt-3</sub>	<i>"This is a picture of a vivid blue background"</i>
Color <sub>prompt-4</sub>	<i>"This is a picture of a vivid colorful background"</i>
Texture <sub>prompt-1</sub>	<i>"This is a picture of textures in the background"</i>
Texture <sub>prompt-2</sub>	<i>"This is a picture of intricately textured background"</i>
Texture <sub>prompt-3</sub>	<i>"This is a picture of colorful textured background"</i>
Texture <sub>prompt-4</sub>	<i>"This is a photo of distorted textures in the background"</i>
Adversarial	Captions generated from BLIP-2 image to caption.

## A.2 Algorithm

We provide the algorithm (Algo. 1) for our approach of generating adversarial backgrounds by optimizing the textual and visual conditioning of the diffusion model. We also tried to optimize only the conditional embeddings or the latent embeddings, but achieve better attack success rate by optimizing both. Note that for crafting adversarial examples on COCO-DC we use ImageNet trained ResNet-50 classifiers and our adversarial objective is to maximize the feature representation distance between clean and adversarial samples. Furthermore, for introducing desired non-adversarial background changes using the textual description  $\mathcal{T}$ , the optimization of the latent and embedding is not needed.

---

### Algorithm 1 Background Generation

---

**Require:** Conditioning module  $\mathcal{C}$ , Diffusion model  $\epsilon_\theta$ , Autoencoder  $\mathcal{V}$ , CLIP text encoder  $\psi_{\text{CLIP}}$ , image  $\mathcal{I}$ , class label  $\mathbf{y}$ , classifier  $\mathcal{F}_\phi$ , denoising steps  $T$ , guidance scale  $\lambda$ , attack iterations  $N$ , and learning rate  $\beta$  for AdamW optimizer  $\mathcal{A}$ .

1: Get the textual and visual conditioning from the image  $\mathcal{I}$

$$\mathcal{C}(\mathcal{I}, \mathbf{y}) = \mathcal{T}_B, \mathcal{M}$$

2: Modify  $\mathcal{T}_B$  to  $\mathcal{T}$  for desired background change.

3: Map the mask  $\mathcal{M}$  and image  $\mathcal{I}$  to latent space:  $i, m \leftarrow \mathcal{V}_{\text{ENC}}(\mathcal{I}, \mathcal{M})$

4: Get the embedding of the textual discription  $\mathcal{T}$ :  $e_{\mathcal{T}} \leftarrow \psi_{\text{CLIP}}(\mathcal{T})$

5: Randomly initialize the latent  $z_T$

6: Get the denoised latent  $z_t$  at time step  $t$ .

7: **for**  $n \in [1, 2, \dots N]$  **do**

8:   **for**  $t \in [t, t + 1, \dots T]$  **do**

9:      $\hat{\epsilon}_\theta^t(z_t, e_{\mathcal{T}}, i, m) = \epsilon_\theta^t(z_t, i, m) + \lambda (\epsilon_\theta^t(z_t, e_{\mathcal{T}}, i, m) - \epsilon_\theta^t(z_t, i, m))$

10:     From noise estimate  $\hat{\epsilon}_\theta$  get  $z_{t-1}$ .

11:   **end for**

12:   Project the latents to pixel space:  $\mathcal{I}_{adv} \leftarrow \mathcal{V}_{\text{DEC}}(z_0)$

13:   Compute Adversarial Loss:

$$\mathcal{L}_{adv} = \mathcal{L}_{CE}(\mathcal{F}_\phi(\mathcal{I}_{adv}), \mathbf{y})$$

14:   Update  $z_t$  and  $e_{\mathcal{T}}$  using  $\mathcal{A}$  to maximize  $\mathcal{L}_{adv}$ :

$$z_t, e_{\mathcal{T}} \leftarrow \mathcal{A}(\nabla_{z_t} \mathcal{L}_{adv}, \nabla_{e_{\mathcal{T}}} \mathcal{L}_{adv})$$

15: **end for**

16: \_\_\_\_\_

17: Generate Adversarial image  $\mathcal{I}_{adv}$  using updated  $z_t$  and  $e_{\mathcal{T}}$ .

---



### A.3 Object Distortion in LANCE

In [45], LANCE method is proposed, which is closely relevant to our approach. LANCE leverages the capabilities of language models to create textual prompts, facilitating diverse image alterations using the prompt-to-prompt image editing method [23] and null-text inversion [42] for real image editing. However, this reliance on prompt-to-prompt editing imposes constraints, particularly limiting its ability to modify only specific words in the prompt. Such a limitation restricts the range of possible image transformations. Additionally, the global nature of their editing process poses challenges in preserving object semantics during these transformations. In contrast, our method employs both visual and textual conditioning, effectively preserving object semantics while generating varied background changes. This approach aligns well with our goal of studying object-to-background context. We use open-sourced code from LANCE to compare it against our approach both quantitatively and qualitatively. We use a subset of 1000 images, named **ImageNet-B<sub>1000</sub>**, for comparison. We observe that our natural object-to-background changes including color and texture perform favorably against LANCE, while our adversarial object-to-background changes perform significantly better as shown in the Table 1. Since LANCE relies on global-level image editing, it tends to alter the object semantics and distort the original object shape in contrast to our approach which naturally preserves the original object and alters the object-to-background composition only. This can be observed in qualitative examples provided in Figures 9 and 10. We further validate this effect by masking the background of original and LANCE-generated counterfactual images. As reported in Table 7, when the background is masked in LANCE-generated counterfactual images, overall accuracy drops from 84.35% to 71.57%. This drop in accuracy compared to original images with masked background, shows that the LANCE framework has distorted the original object semantics during optimization. In contrast to this, our proposed approach allows us to study the correlation of object-to-background compositional changes without distorting the object semantics.

**Table 7:** Performance evaluation and comparison on **ImageNet-B<sub>1000</sub>** dataset. The drop in accuracy of LANCE dataset when the background is masked clearly highlight the image manipulation being done on the object of interest.

Dataset	Masked Background							Average
	ViT-T	ViT-S	Swin-T	Swin-S	Res-50	Res-152	Dense-161	
Original	70.5	86.1	84.2	87.6	87.2	91.2	83.7	84.35
LANCE	59.5	72.5	72.3	75.3	71.9	77.5	72.0	71.57

#### A.4 Qualitative Comparison with Related Works

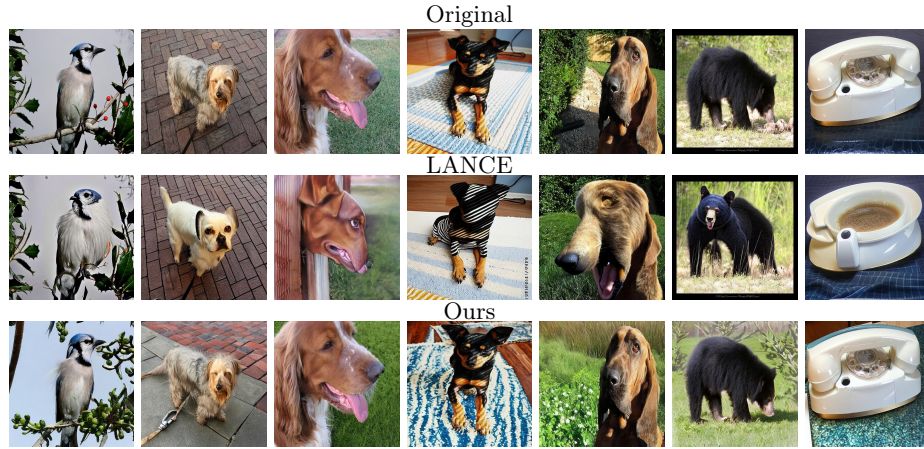


**Fig. 9:** Background Compositional changes on **ImageNet-B<sub>1000</sub>** dataset using LANCE and our method. LANCE fails to preserve object semantics, while our method exclusively edits the background.

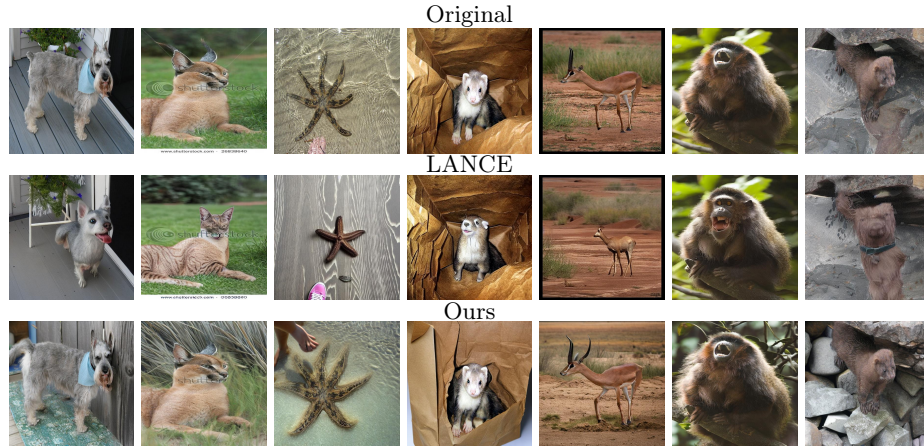


**Fig. 10:** Background Compositional changes on **ImageNet-B<sub>1000</sub>** dataset using LANCE and our method. LANCE fails to preserve object semantics, while our method exclusively edits the background.

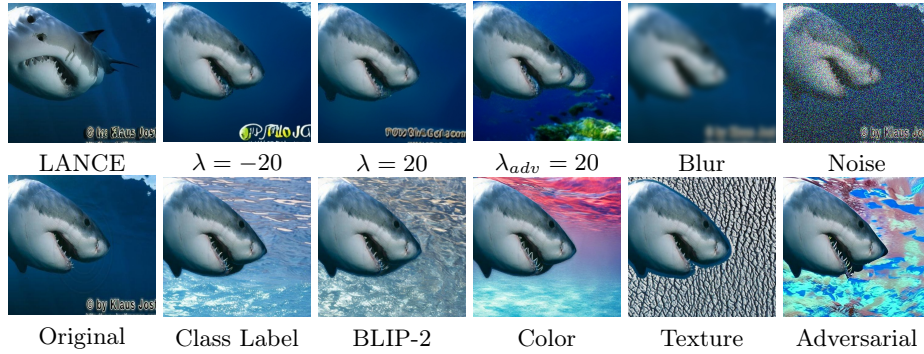


**Fig. 11:** Qualitative comparison of our background changes (*bottom row*) with previous related work (*top row*). Our method enables diversity and controlled background edits.

### A.5 Ablation on Background Changes

In this section, we report results on **ImageNet-B** and **COCO-DC** for uni-modal classifiers in Table 8 and Table 9 reports zero-shot classification results on **ImageNet-B**. Furthermore, ablations across diverse color and texture prompts is provided in Table 10 and 11.

**Table 8:** Resilience of Transformer and CNN models trained on ImageNet and COCO training sets against our proposed object-to-background context variations. We report top-1 (%) accuracy. We observe that CNN-based models are relatively more robust than Transformers.

Datasets	Background	Transformers				CNN			Average
		ViT-T	ViT-S	Swin-T	Swin-S	Res-50	Res-152	Dense-161	
ImageNet-B	Original	96.04	98.18	98.65	98.84	98.65	99.27	98.09	98.25
	Class label	92.82	94.75	96.18	96.55	97.24	97.56	95.8	95.84 <sub>(-2.41)</sub>
	BLIP-2 Caption	86.77	90.41	92.71	93.60	94.46	95.35	91.62	92.13 <sub>(-6.12)</sub>
	Color	70.64	84.52	86.84	88.84	89.44	92.89	83.19	85.19 <sub>(-13.06)</sub>
	Texture	68.24	79.73	81.09	84.41	83.21	87.66	77.29	80.23 <sub>(-18.02)</sub>
ImageNet-B <sub>1000</sub>	Original	95.01	97.50	97.90	98.30	98.50	99.10	97.20	97.64
	Adversarial	18.40	32.10	25.00	31.70	2.00	28.00	14.40	21.65 <sub>(-75.99)</sub>
COCO-DC	Original	82.96	86.24	88.55	90.23	88.55	89.08	86.77	87.21
	BLIP-2 Caption	82.69	84.73	86.24	86.95	88.46	86.69	85.01	85.67 <sub>(-1.54)</sub>
	Color	55.54	61.04	70.09	72.13	74.97	75.10	66.19	66.66 <sub>(-20.55)</sub>
	Texture	52.52	58.82	68.05	70.09	70.71	74.77	63.79	63.99 <sub>(-23.22)</sub>
	Adversarial	49.68	55.72	61.93	69.12	55.45	61.13	57.76	58.68 <sub>(-28.52)</sub>

**Table 9:** Comparative Evaluation of Zero-shot CLIP and Eva CLIP Vision-Language Models on **ImageNet-B** and **ImageNet-B<sub>1000</sub>**. Top-1(%) accuracy is reported. We find that Eva CLIP models showed more robustness in all object-to-background variations.

Datasets	Background	CLIP							Average
		ViT-B/32	ViT-B/16	ViT-L/14	Res50	Res101	Res50x4	Res50x16	
<b>ImageNet-B</b>	Original	75.56	81.56	88.61	73.06	73.95	77.87	83.25	79.12
	Class label	80.83	84.41	89.41	78.87	79.33	81.94	85.67	82.92(+3.80)
	BLIP-2 Captions	69.33	73.66	79.07	67.44	68.70	71.55	75.78	72.22(-6.90)
	Color	53.02	63.08	71.42	53.53	55.87	60.05	71.28	61.18(-17.94)
	Texture	51.01	62.25	69.08	51.35	53.46	61.10	70.33	59.79(-19.33)
<b>ImageNet-B<sub>1000</sub></b>	Original	73.90	79.40	87.79	70.69	71.80	76.29	82.19	77.43
	Adversarial	25.5	34.89	48.19	18.29	24.40	30.29	48.49	32.87(-46.25)

Datasets	Background	EVA-CLIP							Average
		g/14	g/14+	B/16	L/14	L/14+	E/14	E/14+	
<b>ImageNet-B</b>	Original	90.80	93.71	90.24	93.71	93.69	95.38	95.84	93.34
	Class label	90.48	93.53	90.20	93.47	93.49	94.78	95.18	93.02(-0.32)
	BLIP-2 Caption	80.56	85.23	81.88	85.28	86.24	88.13	88.68	85.14(-8.20)
	Color	77.25	83.96	76.24	83.63	85.79	88.70	88.33	83.41(-9.93)
	Texture	75.93	82.76	74.44	82.56	86.35	87.84	88.44	82.62(-10.72)
<b>ImageNet-B<sub>1000</sub></b>	Original	88.80	92.69	89.19	91.10	91.99	93.80	94.60	91.74
	Adversarial	55.59	62.49	48.70	65.39	73.59	70.29	73.29	64.19(-27.55)

**Table 10:** Performance evaluation of naturally trained classifiers and zero-shot CLIP models on **ImageNet-B**. The text prompts used for color and texture changes are provided in Table 6.

Background	Naturally Trained Models							
	ViT				CNN			Average
	ViT-T	ViT-S	Swin-T	Swin-S	ResNet50	ResNet152	DenseNet	
Clean	96.04	98.18	98.65	98.84	98.65	99.27	98.09	98.25
Color <sub>prompt-1</sub>	76.58	86.43	88.92	91.23	91.08	93.79	86.05	87.72
Color <sub>prompt-2</sub>	77.09	87.57	89.33	90.99	90.62	93.40	86.61	87.94
Color <sub>prompt-3</sub>	76.80	86.97	88.74	90.99	90.62	93.18	87.41	87.82
Color <sub>prompt-4</sub>	70.64	84.52	86.84	88.84	89.44	92.89	83.19	85.19
Texture <sub>prompt-1</sub>	79.07	87.92	90.17	91.68	91.18	94.42	88.28	88.96
Texture <sub>prompt-2</sub>	75.29	85.84	87.74	90.32	89.01	93.04	84.77	86.57
Texture <sub>prompt-3</sub>	67.97	82.54	86.17	87.99	87.99	91.28	82.99	83.85
Texture <sub>prompt-4</sub>	68.24	79.73	81.09	84.41	83.21	87.66	77.29	80.23

Background	CLIP Models							
	ViT				CNN			Average
	ViT-B/32	ViT-B/16	ViT-L/14	ResNet50	ResNet101	ResNet50x4	ResNet50x16	
Clean	75.56	81.56	88.61	73.06	73.95	77.87	83.25	79.12
Color <sub>prompt-1</sub>	58.32	65.54	72.75	57.43	60.92	65.97	73.04	64.49
Color <sub>prompt-2</sub>	57.91	67.28	74.44	58.67	60.12	65.9	74.13	65.49
Color <sub>prompt-3</sub>	57.27	66.77	74.07	57.89	59.03	66.10	74.06	65.03
Color <sub>prompt-4</sub>	53.02	63.08	71.42	53.53	55.87	60.05	71.28	61.18
Texture <sub>prompt-1</sub>	59.05	68.50	75.67	60.38	61.78	66.99	74.31	66.67
Texture <sub>prompt-2</sub>	58.60	68.01	74.40	58.29	59.56	66.34	74.67	65.69
Texture <sub>prompt-3</sub>	52.89	64.30	68.70	53.29	55.35	61.58	69.35	60.78
Texture <sub>prompt-4</sub>	51.01	62.25	69.08	51.35	53.46	61.10	70.33	59.79

**Table 11:** Performance evaluation of naturally trained classifiers on COCO-DC dataset. The text prompts used for color and texture changes are provided in Table 6.

Background	ViT				CNN		Average
	ViT-T	ViT-S	Swin-T	Swin-S	ResNet50	Dense-161	
Clean	82.96	86.24	88.55	90.23	88.55	86.77	87.21
Color <sub>prompt-1</sub>	61.66	65.92	73.38	73.73	75.86	71.6	70.35
Color <sub>prompt-2</sub>	64.86	70.01	76.84	77.10	77.81	75.06	73.61
Color <sub>prompt-3</sub>	62.64	67.52	73.29	74.09	77.28	73.64	71.41
Color <sub>prompt-4</sub>	55.54	61.04	70.09	72.13	74.97	66.19	66.66
Texture <sub>prompt-1</sub>	67.96	70.36	75.42	78.70	79.94	73.55	74.32
Texture <sub>prompt-2</sub>	63.97	69.56	74.62	77.72	78.97	75.15	73.33
Texture <sub>prompt-3</sub>	52.52	58.82	68.05	70.09	70.71	63.79	63.99
Texture <sub>prompt-4</sub>	56.16	61.57	66.72	70.18	69.56	67.25	65.24

## A.6 Evaluation on Adversarially Trained models

In this section, we evaluate adversarially trained Res-18, Res-50, and Wide-Res-50 models across background changes induced by our methods and baseline methods (See Table 12, 13, and 14).

**Table 12:** Performance evaluation and comparison of our dataset with state of the art methods on adversarially trained Res-18 models. The images are generated on ImageNet-B<sub>1000</sub> dataset. We report top-1 average accuracy of models trained on various adversarial budget.

Datasets	$\ell_\infty$				$\ell_2$			
	$\epsilon=0.5$	$\epsilon=2.0$	$\epsilon=4.0$	$\epsilon=8.0$	$\epsilon=0.5$	$\epsilon=2.0$	$\epsilon=4.0$	$\epsilon=8.0$
Original	88.00	78.30	69.70	54.40	84.60	81.40	68.80	57.50
ImageNet-E ( $\lambda=-20$ )	84.50	77.01	69.10	54.80	83.40	80.00	68.80	59.00
ImageNet-E ( $\lambda=20$ )	81.41	74.94	66.36	52.52	81.61	75.75	65.65	55.05
ImageNet-E ( $\lambda_{adv}=20$ )	75.15	66.16	56.36	45.35	72.82	66.66	55.75	45.05
LANCE	76.37	66.78	59.13	45.17	74.99	73.19	61.60	48.68
Class label	87.10	79.90	69.40	57.30	85.00	79.90	70.90	57.80
BLIP-2 Caption	80.90	73.10	67.10	51.00	79.50	75.30	63.10	53.40
Color	56.90	45.80	35.40	25.70	53.20	46.80	32.80	23.40
Texture	59.20	47.10	38.60	28.70	54.30	48.10	35.50	26.20
Adversarial	12.10	19.80	24.60	26.80	10.90	12.40	16.90	17.20

**Table 13:** Performance evaluation and comparison of our dataset with state of the art methods on adversarially trained Res-50 models. The images are generated on **ImageNet-B<sub>1000</sub>** dataset. We report top-1 average accuracy of models trained on various adversarial budget.

Datasets	$\ell_\infty$				$\ell_2$			
	$\varepsilon=0.5$	$\varepsilon=2.0$	$\varepsilon=4.0$	$\varepsilon=8.0$	$\varepsilon=0.5$	$\varepsilon=2.0$	$\varepsilon=4.0$	$\varepsilon=8.0$
Original	95.20	89.30	83.20	72.40	94.30	91.10	80.90	70.80
ImageNet-E ( $\lambda=-20$ )	93.10	89.20	82.00	70.70	91.70	88.50	79.60	69.10
ImageNet-E ( $\lambda=20$ )	92.52	86.36	80.60	67.97	90.40	86.96	76.26	68.08
ImageNet-E ( $\lambda_{adv} = 20$ )	84.44	78.78	71.71	58.58	80.50	76.76	65.75	56.86
LANCE	81.94	78.96	70.11	59.72	83.52	80.46	69.83	61.32
Class label	92.40	88.50	82.70	72.50	90.70	88.60	80.20	70.50
BLIP-2 Caption	87.90	83.70	79.00	67.90	86.60	84.60	73.70	65.70
Color	70.80	60.30	53.20	39.50	67.20	58.50	44.40	34.20
Texture	69.70	61.00	54.60	43.40	64.90	59.70	48.00	37.70
Adversarial	10.80	17.10	18.10	16.60	10.70	11.90	14.70	13.40

**Table 14:** Performance evaluation and comparison of our dataset with state of the art methods on adversarially trained Wide Res-50 models. The images are generated on **ImageNet-B<sub>1000</sub>** dataset. We report top-1 average accuracy of models trained on various adversarial budget.

Datasets	$\ell_\infty$				$\ell_2$			
	$\varepsilon=0.5$	$\varepsilon=2.0$	$\varepsilon=4.0$	$\varepsilon=8.0$	$\varepsilon=0.5$	$\varepsilon=2.0$	$\varepsilon=4.0$	$\varepsilon=8.0$
Original	96.20	92.60	89.10	78.70	95.60	94.00	87.00	78.30
ImageNet-E ( $\lambda=-20$ )	94.10	91.10	86.60	76.40	93.20	91.60	84.20	76.90
ImageNet-E ( $\lambda=20$ )	92.82	89.29	83.53	75.15	91.21	88.68	81.11	73.63
ImageNet-E ( $\lambda_{adv} = 20$ )	87.17	76.56	66.16	82.92	82.22	82.00	71.41	62.42
LANCE	84.18	81.34	77.07	64.51	83.48	83.09	77.40	66.09
Class label	93.50	90.60	87.30	78.80	92.10	90.80	83.70	75.50
BLIP-2 Caption	90.20	86.20	82.80	74.30	88.90	86.70	80.00	69.20
Color	72.2	66.60	60.70	51.20	68.10	65.10	51.40	40.90
Texture	73.80	66.70	61.70	53.60	67.20	64.60	52.00	44.20
Adversarial	13.90	22.90	28.00	32.00	12.40	15.10	19.50	20.60



### A.7 Evaluation on Recent Vision Models

We have conducted experiments on recent transformer CNN based models like DeiT [59] and ConvNeXt [38], and their results are presented in Table 15. We observe a consistent trend in model performance on our dataset, revealing that even the modern vision models are vulnerable to background changes.

**Table 15:** Performance evaluation on naturally trained classifiers on **ImageNet-B** and **ImageNet-B<sub>1000</sub>** dataset. All models exhibit a marked decrease in accuracy when the background is modified, highlighting their sensitivity to changes in the environment. The decline in performance is minimal with class label backgrounds but more pronounced with texture and color alterations. The most significant accuracy drop occurs under adversarial conditions, underscoring the substantial challenge posed by such backgrounds to the classifiers.

Datasets	Background	Transformers				CNN			
		DeiT-T	DeiT-S	DeiT-B	Average	ConvNeXt-T	ConvNeXt-B	ConvNeXt-L	Average
ImageNet-B	Original	96.36	99.27	99.41	98.34	99.07	99.21	99.40	99.22
	Class label	94.18	96.85	97.74	96.25	97.60	97.51	97.51	97.54
	BLIP-2 Caption	89.33	94.29	95.07	92.89	94.64	94.82	95.47	94.97
	Color	80.96	89.48	91.11	87.13	92.11	93.58	93.58	93.09
	Texture	74.15	84.01	86.75	81.63	88.50	89.50	91.13	89.71
ImageNet-B <sub>1000</sub>	Original	95.44	99.10	99.10	97.88	99.00	99.00	92.92	96.97
	Adversarial	20.40	29.62	34.81	28.27	32.88	42.52	48.60	41.33

### A.8 Evaluation on DINOv2 models

Our findings underscore the necessity of training vision models to prioritize discriminative and salient features, thereby diminishing their dependence on background cues. Recent advancements, such as the approaches by [54] employing a segmentation backbone for classification to improve adversarial robustness and by [9] using additional learnable tokens known as *registers* for interpretable attention maps, resonate with this perspective. Our preliminary experiments with the DINOv2 models [44], as presented in Table 16, corroborate this hypothesis. Across all the experiments, models with registers (*learnable tokens*) provide more robustness to background changes, with significant improvement seen in the adversarial background changes.

**Table 16:** Performance comparison of classifiers that are trained different on **ImageNet-B** dataset. The DINOv2 model with registers generally shows higher robustness to background changes, particularly in the presence of color, texture and adversarial backgrounds. This suggests that the incorporation of registers in DINOv2 enhances its ability to maintain performance despite challenging background alterations.

Dataset	Background	Dinov2				Dinov2 <b>registers</b>			
		ViT-S	ViT-B	ViT-L	Average	ViT-S	ViT-B	ViT-L	Average
ImageNet-B	Original	96.78	97.18	98.58	97.51	97.71	98.05	99.14	98.30
	Class label	94.62	96.02	97.18	95.94	95.55	96.44	97.94	96.64
	BLIP-2 Caption	89.22	91.73	94.33	91.76	90.86	92.10	95.02	92.66
	Color	83.85	89.68	93.31	88.94	85.88	91.15	94.64	90.55
	Texture	83.63	89.08	92.44	88.38	84.98	91.03	93.97	89.99
ImageNet-B <sub>1000</sub>	Original	95.12	96.50	98.10	96.57	97.91	97.80	99.00	98.23
	Adversarial	54.31	71.62	80.87	68.93	58.30	76.21	84.50	73.00

A.9 Vision Language model for Image Captioning



**Fig. 12:** A visual comparison of BLIP-2 captions on clean and generated datasets. The top row shows captions on clean images, while the bottom row displays captions on generated images. As background complexity increases, BLIP-2 fails to accurately represent the true class in the image.

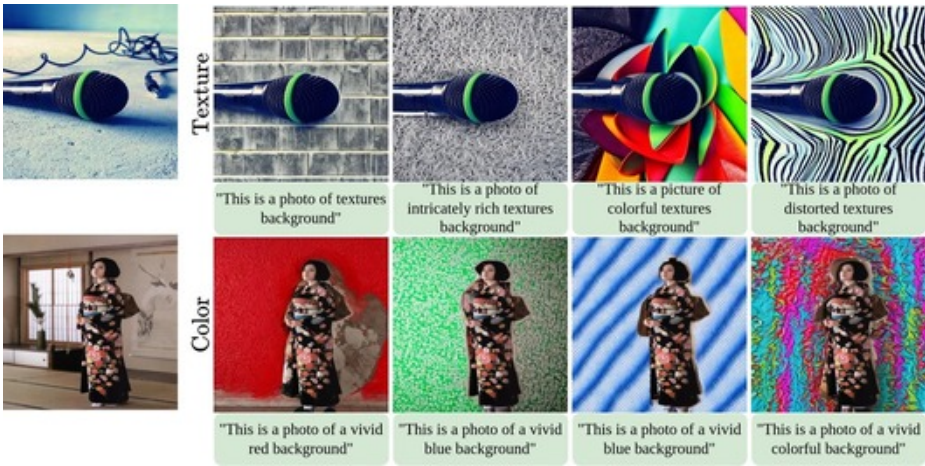


**Fig. 13:** The figure illustrates the introduction of background variations achieved through a diverse set of texture and color text prompts

## A.10 Qualitative Results on Detection

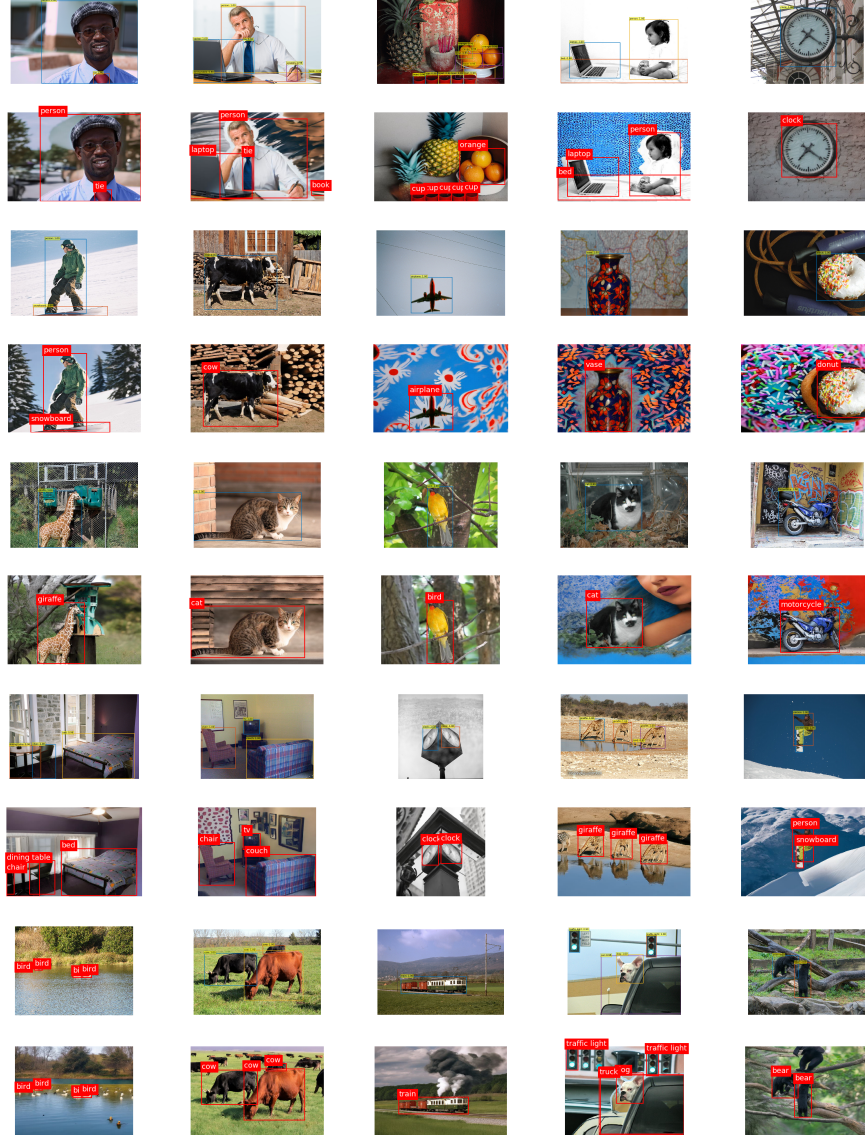


**Fig. 14:** We use diverse prompts to capture the diverse background shifts on samples from COCO-DC. The figure illustrate a comparison of prediction of Mask-RCNN on both clean and generated samples on COCO-DC. Each two adjacent rows represents the prediction of Mask-RCNN on clean (*top*) and generated images (*bottom*).

### A.11 Effect of Background Change on Segmentation Models

Figure 15, 16, and 17 provide failure cases of FastSAM to correctly segment the object in the images where background has been changed in terms of color, texture, and adversarial, respectively. Since we obtain the object masks for **ImageNet-B** using FastSAM, we compare those masks using IoU with the ones obtained by FastSAM on the generated dataset (see Table 17).

**Table 17:** IoU distribution of FastSAM. Percentage of images within an IoU range is reported.

Background	0.0-0.2	0.2-0.4	0.4-0.6	0.6-0.8	0.8-1.0
Class Label	8.10	5.93	8.02	13.03	64.92
BLIP-2 Caption	5.70	4.81	6.92	13.01	69.56
Color	1.65	1.39	2.31	4.99	89.65
Texture	2.11	1.02	1.78	4.07	91.02
Adversarial	4.87	2.91	4.32	10.63	77.27

**Table 18:** DETR Object detection evaluation on COCO-DC

Background	Box AP	Recall AR
Original	0.65	0.81
BLIP-2 Caption	0.53	0.76
Color	0.52	0.73
Texture	0.52	0.71
Adversarial	0.42	0.62

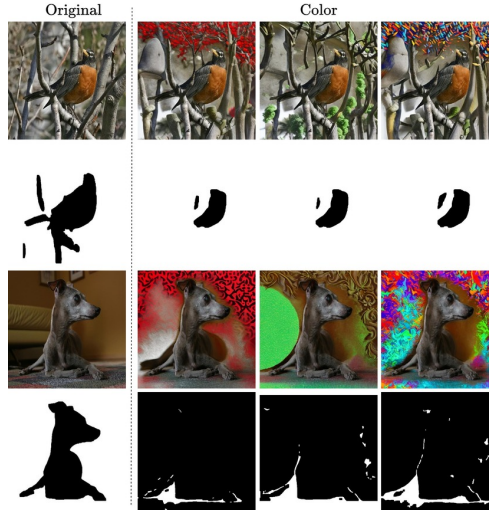


**Fig. 15:** Instances illustrating FastSAM model's failure to accurately segment masks for the background color changes on **ImageNet-B** samples..



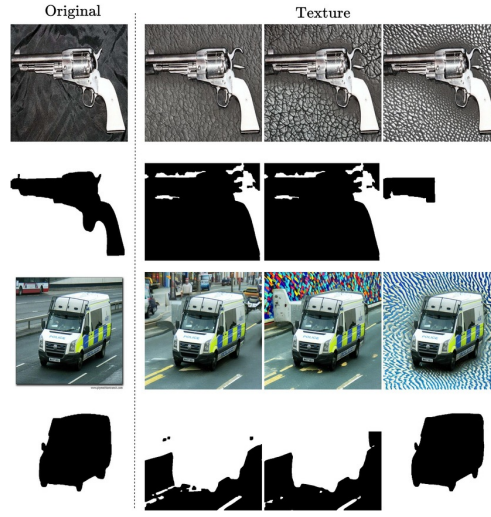


**Fig. 16:** Instances illustrating FastSAM model's failure to accurately segment masks for the background texture changes on *ImageNet-B* samples.

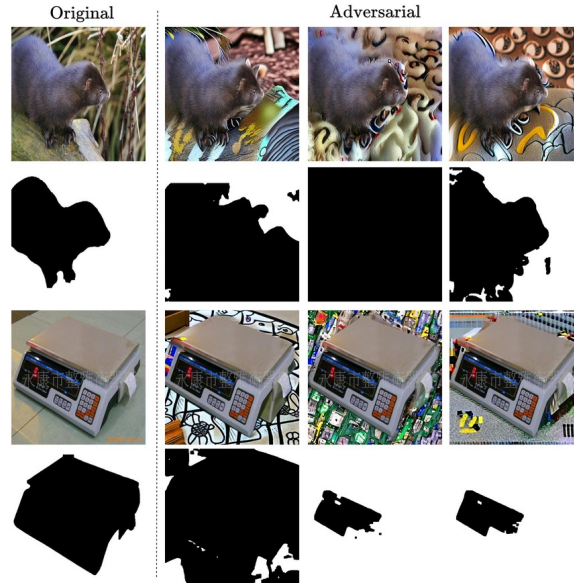


**Fig. 17:** Instances illustrating FastSAM model's failure to accurately segment masks for the adversarial background changes on *ImageNet-B<sub>1000</sub>* samples.

### A.12 Exploring Feature Space of Vision Models

In Figure 18 and 19, we explore the visual feature space of vision and vision language model using t-SNE visualizations. We observe that as the background changes deviate further from the original background, a noticeable shift occurs in the feature space. The distinct separation or clustering of features belonging to the same class appears to decrease. This observation suggests a significant correlation between the model’s decision-making process and the alterations in the background. Furthermore, we also show the GradCAM [51] on generated background changes. We observe that diverse background changes significantly shift the attention of the model as can be seen from Figure 20 and 21.

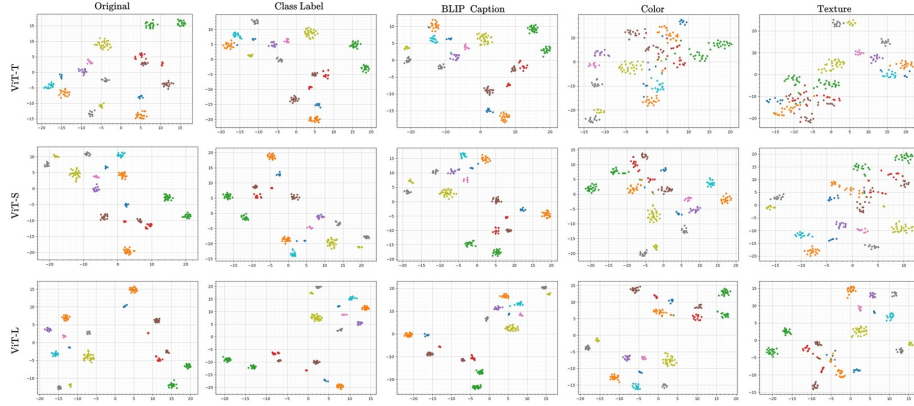


**Fig. 18:** t-SNE visualization of classifier models on ImageNet-B dataset.



**Fig. 19:** t-SNE visualization of CLIP Vision Encoder features on ImageNet-B dataset.



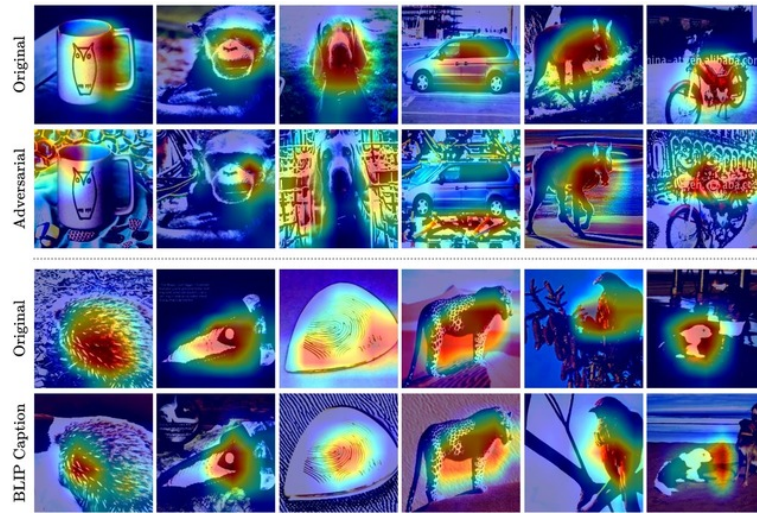


**Fig. 20:** GradCAM [51] visualization of adversarial and BLIP-2 background examples. The activation maps were generated on ImageNet pre-trained Res-50 model.

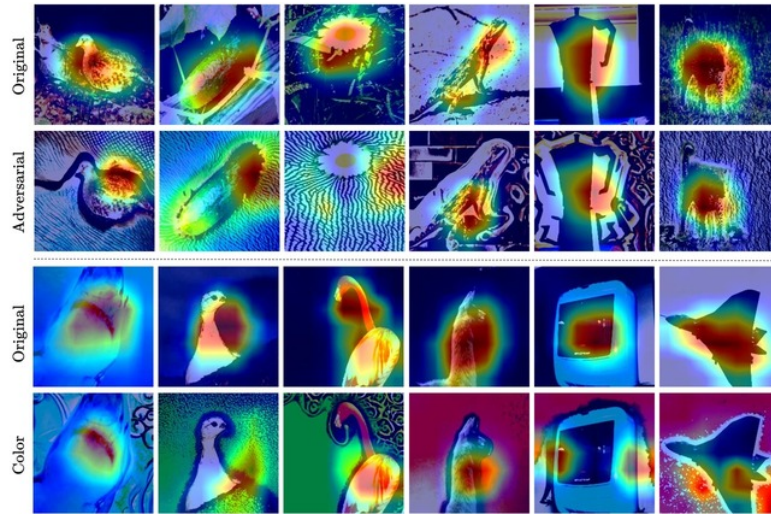


**Fig. 21:** GradCAM [51] visualization of texture and color background changes. The activation maps were generated on ImageNet pre-trained Res-50 model.

### A.13 Diversity and Diffusion parameter ablation

In this section, we qualitatively analyze the diversity in visual results of the diffusion model. In Figure 22, we show that keeping textual and visual guidance fixed, the diffusion model is still able to generate diverse changes with similar background semantics at different seeds for the noise  $z_T$ . Furthermore, we explore the diversity in generating realistic background changes across an original image by using diverse class agnostic textual prompts, capturing different realistic backgrounds. Figure 23 and 24 show some of the qualitative results obtained on **ImageNet-B** samples using prompts generated from ChatGPT). Furthermore, we show the visual examples of color, texture, and adversarial attack on **ImageNet-B** dataset in Figure 25, 26, and 27. We also provide a visualization in Figure 28 showing the effect of changing diffusion model parameters.

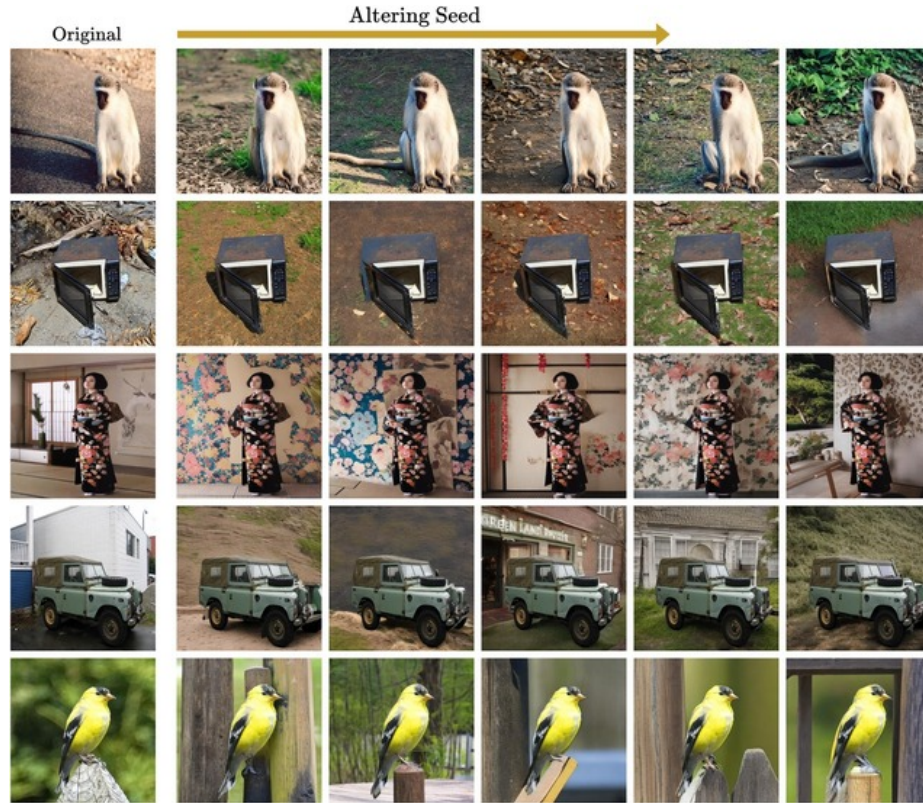


**Fig. 22:** In this figure, examples are generated using BLIP-2 captions by altering the seed from left to right in the row. This highlights the high diversity achievable with the diffusion model when employing different starting noise latents.



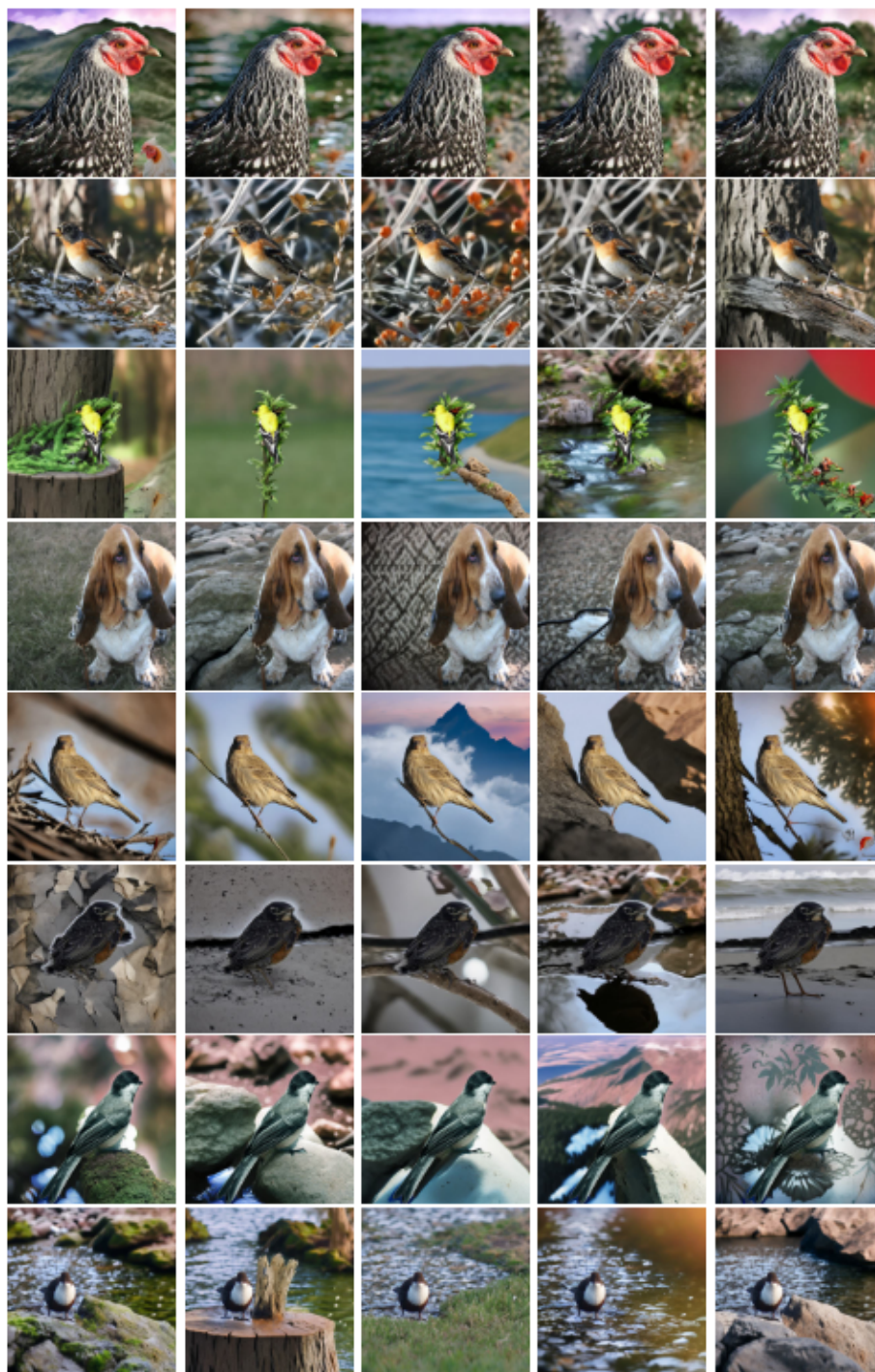


**Fig. 23:** Using diverse prompts to capture for diverse background shifts on samples from ImageNet-B.

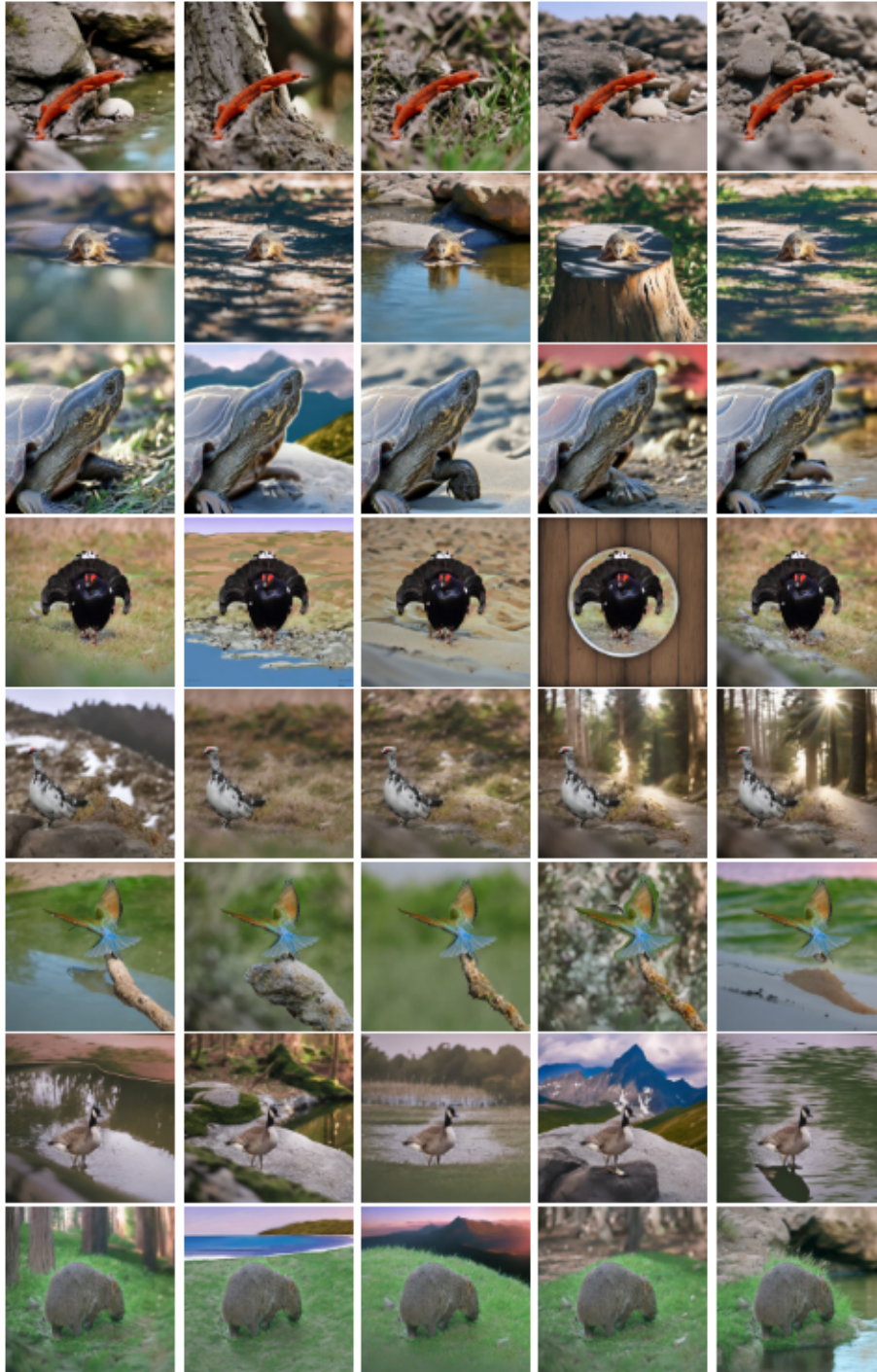


**Fig. 24:** Using diverse prompts to capture for diverse background shifts on samples from ImageNet-B.



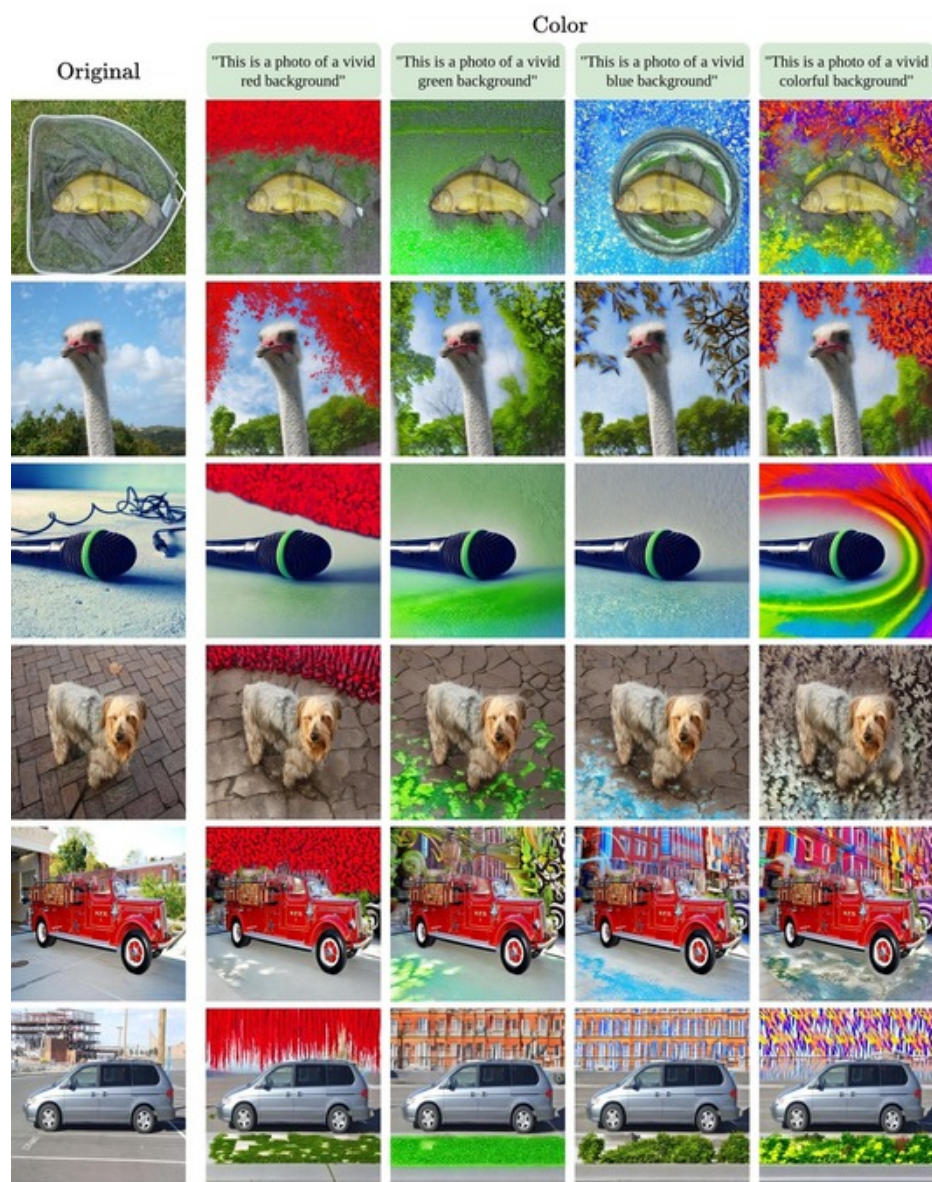


**Fig. 25:** Images generated through diverse color prompts on ImageNet-B.

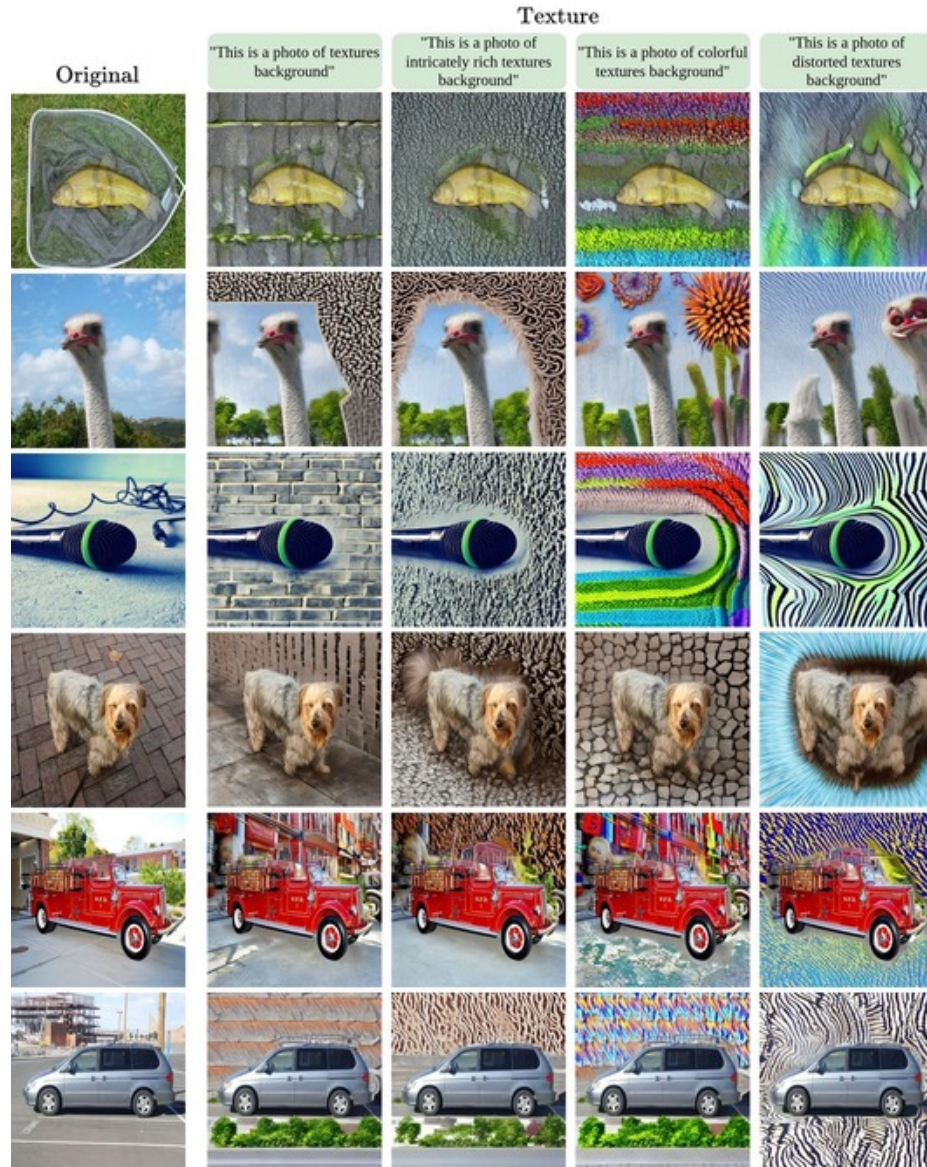


**Fig. 26:** Images generated through diverse texture prompts on ImageNet-B.



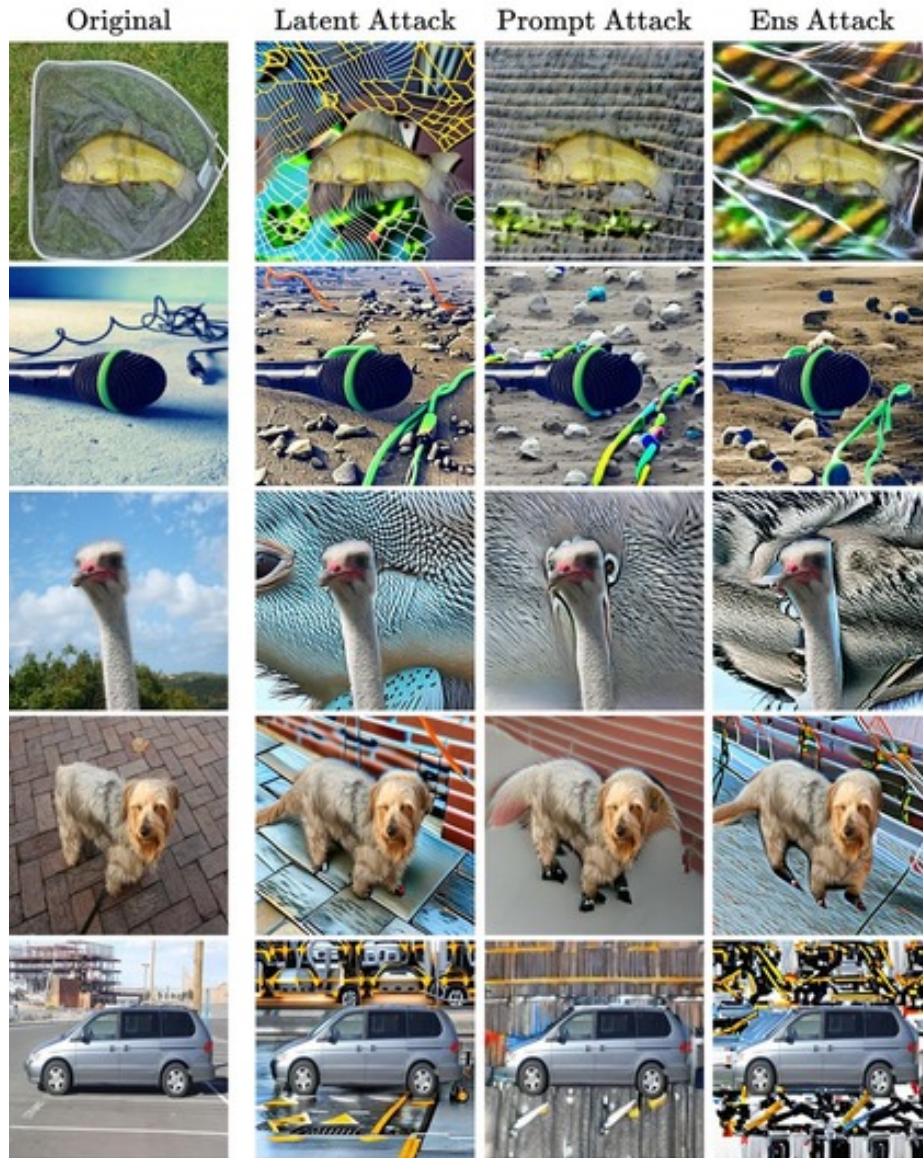


**Fig. 27:** Images generated under various attack scenarios on ImageNet-B<sub>1000</sub>. Here we show the visualization for latent, prompt, and ensemble attack that are generated by optimizing latent, text prompt embeddings, and both respectively.

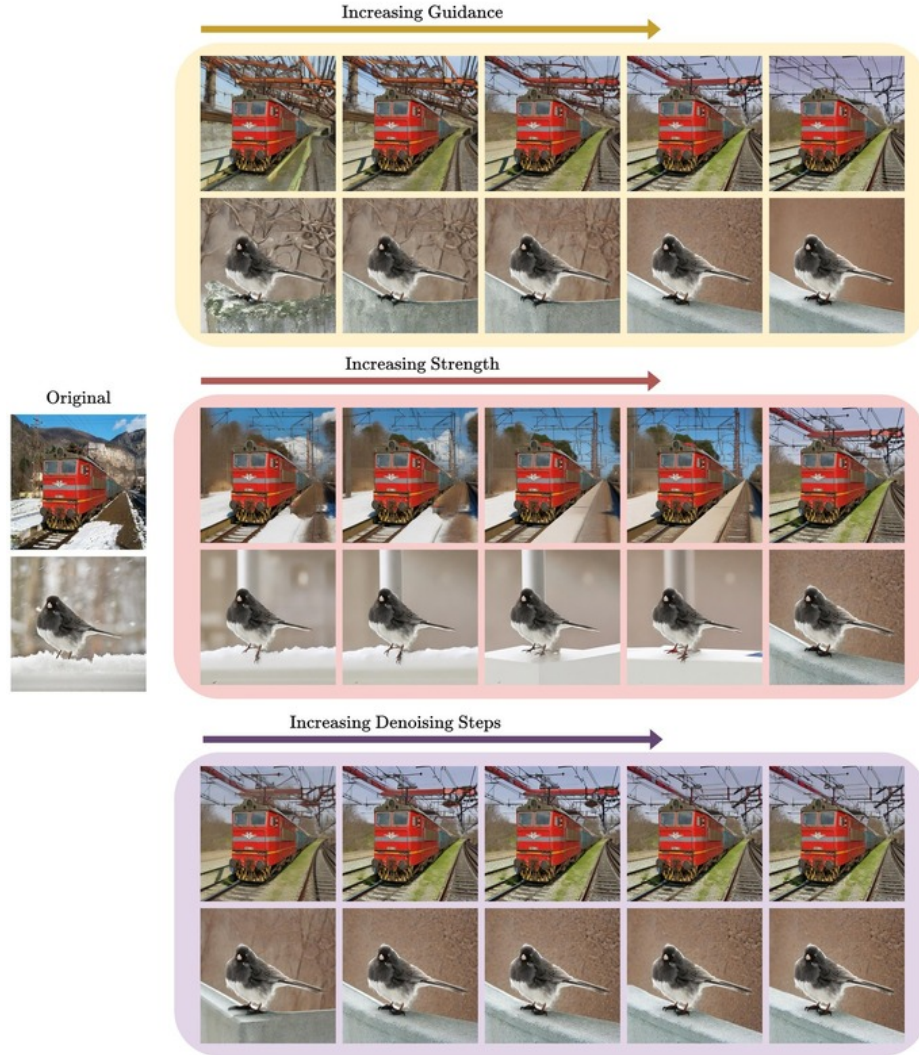


**Fig. 28:** Visualization on samples taken from ImageNet-B. Varying parameters like guidance, strength, and denoising steps while using BLIP-2 caption as the prompt. Increasing guidance leads to more fine-detailed background changes. Additionally, greater strength correlated with more pronounced alterations from the original background. And, augmenting diffusion steps improves image quality.



### A.14 Misclassified Samples

We observe that there exist images which get misclassified (*by ResNet-50*) across several background alterations as can be seen from Figure 29. In Figure 30 we show examples on which the highly robust *EVA-CLIP ViT-E/14+* model fails to classify the correct class. After going through the misclassified samples, we visualize some of the *hard* examples in Figure 32. Furthermore, we also provide visualisation of images misclassified with adversarial background changes in Figure 31.

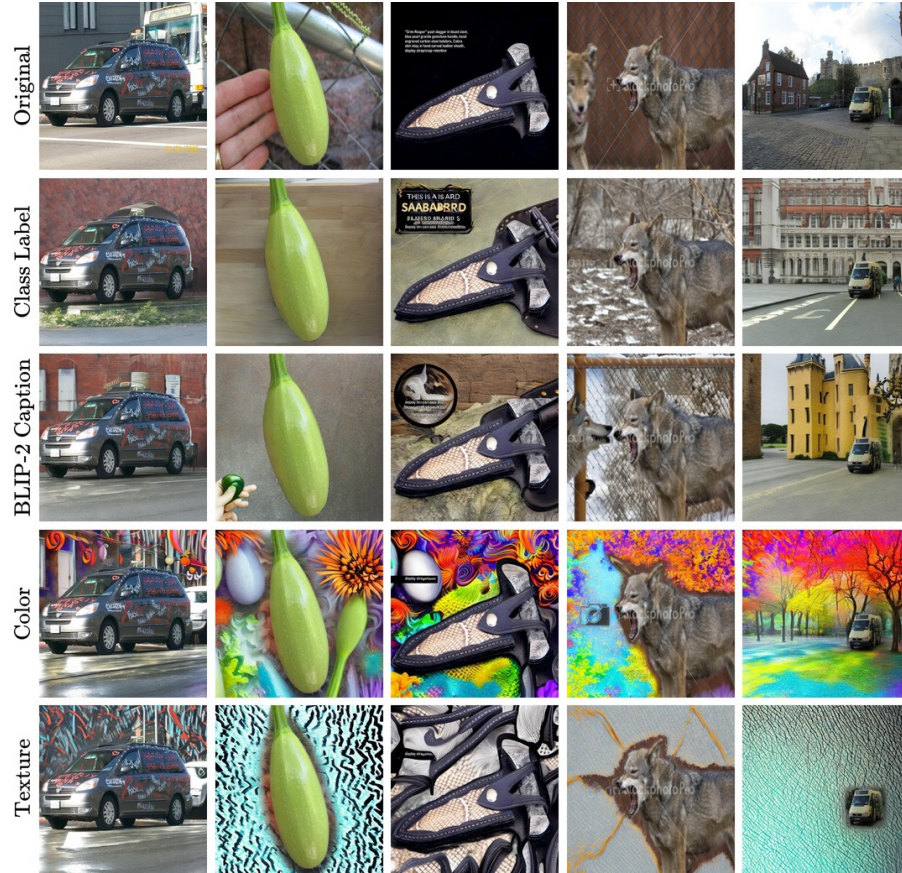


**Fig. 29:** Images misclassified by Res-50 across different background changes

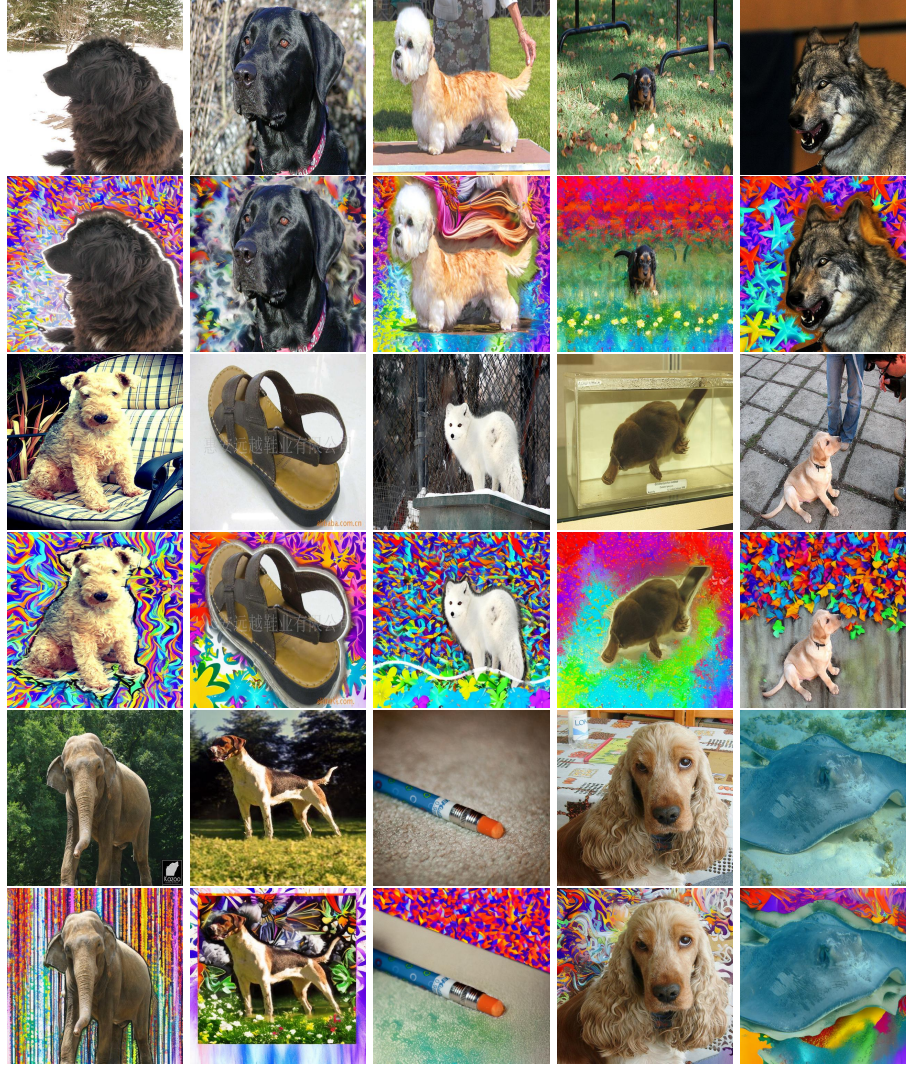


**Fig. 30:** Visual illustration of misclassified samples on color background and corresponding clean image samples. In two adjacent rows, *first row* represent the clean images and the *second row* represent the corresponding colorful background images



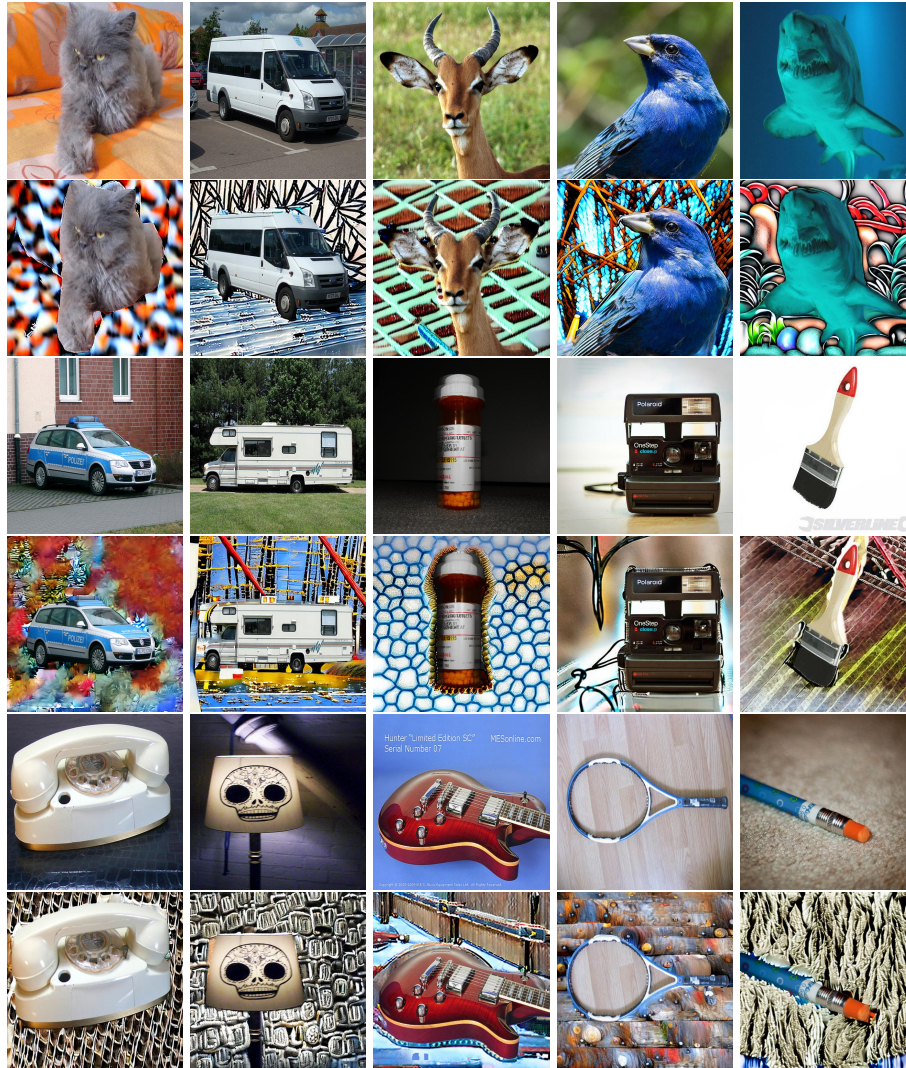


**Fig.31:** Visual illustration of misclassified samples on adversarial background and corresponding clean image samples. In two adjacent rows, *first row* represents the clean images and the *second row* represents the corresponding adversarial images

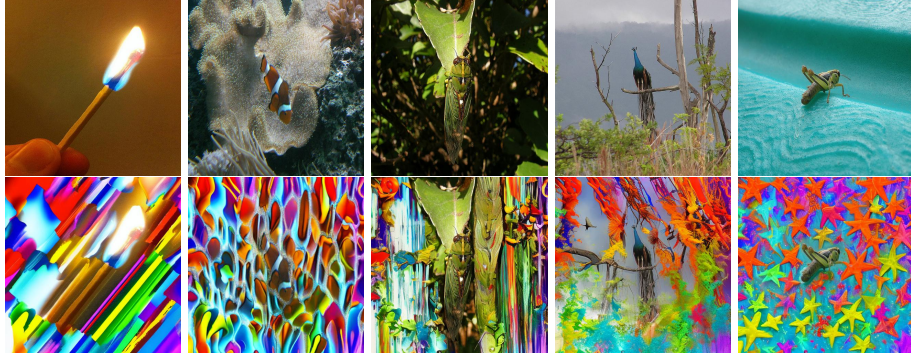


**Fig. 32:** Visual illustration of *hard* samples on color background

### A.15 Limitations and Future Directions

**Limitations:** In Figure 33, we observe that for objects covering a small region in the image, relying solely on the class name to guide the diffusion model can result in alterations of the object shape, expanding the influence of the class name semantics to larger image regions. However, by supplementing with descriptive captions that encompass the object-to-background context, we partially mitigate this effect. Furthermore, the generated textured background can inadvertently camouflage the object. To address this concern, we slightly expand the object mask to clearly delineate the object boundaries.

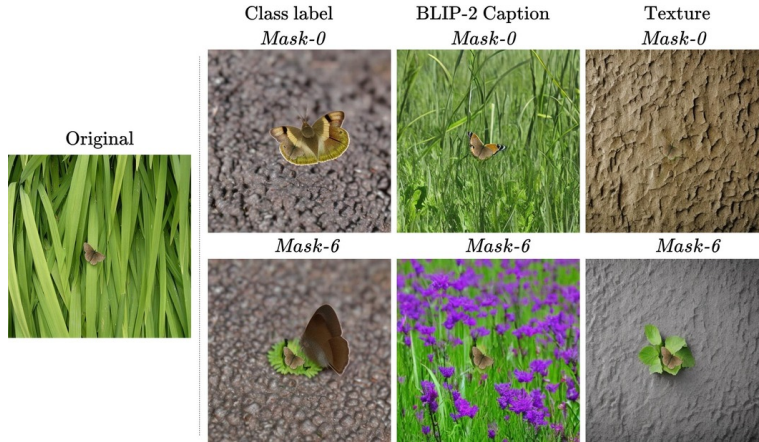


**Fig. 33:** Limitation: Background changes on small objects in the scene. Enlarging the mask (here by 6 pixels) helps in mitigating the issue to some effect.

**Future Directions:** Our current work represents one of the preliminary efforts in utilizing diffusion models to study the object-to-background context in vision-based systems. Based on our observations and analysis, the following are the interesting future directions.

- Since large capacity models in general show better robustness to object-to-background compositions, coming up with new approaches to effectively distill knowledge from these large models could improve how small models cope with background changes. This can improve resilience in small models that can be deployed in edge devices.
- Another direction is to set up object-to-background priors during adversarial training to expand robustness beyond just adversarial changes. To some extent, successful examples are recent works [9, 54] where models are trained to discern the salient features in the image foreground. This leads to better robustness.
- Our work can be extended to videos where preserving the semantics of the objects across the frames while introducing changes to the background temporally will help understand the robustness of video models.
- Additionally, the capabilities of diffusion models can be explored to craft complex changes in the object of interest while preserving the semantic integrity. For instance, in [61], diffusion models are employed to generate multiple viewpoints of the same object. Additionally, in [29], non-rigid motions of objects are created while preserving their semantics. By incorporating these with our approach, we can study how vision models maintain semantic consistency in dynamic scenarios.

### A.16 Potential External Factors

When composing object-to-background change with texture, color, or adversarial patterns, the target models can perceive those as some other class if that pattern or composition is dominant in that class during the training of the models. We discuss the potential external factors and how our proposed method minimizes the effect of those external factors on object-to-background compositional changes.

**Preserving Object Semantics:** We preserve object semantics by using strong visual guidance via SAM for precise object delineation.

**Possibility of extra objects in the Background:** Kindly note that a) we use a pretrained diffusion model that is conditioned on a pretrained CLIP text encoder, this means that the generated output follows the latent space of the CLIP text encoder which is aligned with CLIP visual encoder. Therefore, we can measure the faithfulness of the generated sample w.r.t the textual prompt used to generate it. We can measure this by encoding the generated output and its corresponding text prompt within CLIP latent space. For a given sample, CLIP or EVA-CLIP performs zero-shot evaluation by measuring the similarity between embedding of class templates (e.g. 1000 templates of ImageNet class) with a given image. Thus, if we add the template for a textual prompt used to generate the object-to-background changes, then we can measure its alignment with the background changes. For instance, instead of using a “a photo of a fish” template for zero-shot classification, we add the relevant template that is with background change, such as “a photo of a fish in the vivid colorful background”. In other words, the relevant template represents the object and background change we introduced. We validate this observation on the EVA-CLIP ViT-E/14+, a highly robust model. Using the class templates such as “a photo of a ”, the model achieves 95.84% accuracy on the original images (ImageNet-B dataset), which decreases to 88.33% when our color background changes are applied (see Table 9 in Appendix A.5). However, when using the relevant template, the performance improves to 92.95%, significantly reducing the gap between the performance on the original and color background changes from 7.51% to 2.89%. These results show that accuracy loss from background changes isn’t due to unwanted background objects of other classes. Furthermore, we manually assess 2.89% of misclassified samples (very few samples, see Figure 30 and 32 in Appendix A.14). These can be considered the hardest examples in our dataset. We observe that even in such hard cases the model’s confusion often stemmed from the complex background patterns instead of the addition of unwanted objects. We observe a similar trend in the case of adversarial patterns as well (see Figure 31 in Appendix A.14). b) Another empirical evidence of how our generated output closely follows the given textual prompts can be observed with BLIP-2 Caption of the original image. In this case, object-background change has similar results as compared to original images across different vision models (Table 2 in the main paper).

**Extension of Objects:** As already detailed in Appendix A.15, we encountered challenges when dealing with objects that occupy a small region in the image,

sometimes leading to certain unwanted extensions to objects. To mitigate this, we filtered our dataset to focus on images where the object covers a significant area. Additionally, we slightly expand object masks computed using SAM to better define boundaries and prevent object shape distortion in the background.

The design choices discussed above, such as strong visual guidance and class-agnostic textual guidance, contribute to the well-calibrated results of our study. This indicates that our results using the conventional metrics such as classification accuracy are well calibrated as well in the context of our high quality of generated data as mentioned above. We note that these choices ensure that the models are primarily challenged by diverse changes in the background, rather than being misled by the presence of unwanted objects. This careful approach underlines the reliability of our findings and highlights the specific factors influencing model performance.

### A.17 Dataset Distribution

ImageNet-B dataset comprises a wide variety of objects belonging to different classes, as illustrated in Figure 34. Our dataset maintains a clear distinction between the background and objects, achieved through a rigorous filtering process applied to the ImageNet validation dataset. Additionally, we provide the list of prompts in Table 6 utilized for the experiments.



**Fig. 34:** Our ImageNet-B dataset encompasses a diverse variety of images spanning 582 distinct classes. In this illustration, we showcase images distribution among all the classes. The figure is plotted in decreasing order of images present in each class.



### A.18 Evaluation on Background/Foreground Images

In this section, we systematically evaluate vision-based models by focusing on background and foreground elements in images. This evaluation involves masking the background of the original image, allowing us to assess the model’s performance in recognizing and classifying the foreground without any cues from the background context. Conversely, we also mask the object or foreground from the image. This step is crucial to understand to what extent the models rely on background information for classifying the image into a specific class. This dual approach provides a comprehensive insight into the model’s capabilities in image classification, highlighting its reliance on foreground and background elements.

**Table 19:** Evaluation of Zero-shot CLIP Models on **ImageNet-B** dataset while masking the object or the background of the image. Top-1(%) accuracy is reported. The accuracy drop is observe when we remove the object clues from the background such as in texture or color background

Background	Foreground							Average
	Res50	Res101	Res50x4	Res50x16	ViT-B/32	ViT-B/16	ViT-B/14	
Original	54.76	58.89	64.86	70.80	59.47	69.42	79.12	65.33
	Background							Average
	Res50	Res101	Res50x4	Res50x16	ViT-B/32	ViT-B/16	ViT-B/14	
Original	15.84	17.74	18.47	20.67	17.72	21.28	28.99	20.10
Class label	27.17	29.08	33.02	35.93	31.35	38.74	46.88	34.59
BLIP-2 Caption	19.05	21.39	23.37	24.57	22.39	27.21	34.42	24.62
Color	3.92	5.46	5.64	6.53	5.64	6.95	10.28	6.34
Texture	3.65	5.12	5.12	5.84	5.43	6.68	10.04	5.98

**Table 20:** DINOv2 model evaluation by masking either the object or the background within the **ImageNet-B** dataset. The integration of the additional token in the DINOv2 model proves beneficial, contributing to enhanced accuracy. However, our observations reveal that these models remain susceptible to background cues, particularly evident in class labels and the BLIP-2 Caption dataset. Interestingly, as we transition towards more generic texture or color backgrounds, a discernible drop in accuracy is observed.

Background	Foreground							Average
	ViT-S	ViT-B	ViT-L	Average	ViT-S <sub>reg</sub>	ViT-B <sub>reg</sub>	ViT-L <sub>reg</sub>	
Original	88.73	93.86	94.89	92.49	96.34	89.95	97.25	94.51
	Background							Average
	ViT-S	ViT-B	ViT-L	Average	ViT-S <sub>reg</sub>	ViT-B <sub>reg</sub>	ViT-L <sub>reg</sub>	
Original	27.72	37.78	51.44	38.98	30.10	42.08	55.18	42.45
Class label	42.70	54.73	66.68	54.70	46.88	58.81	68.97	58.22
BLIP-2 Caption	30.51	40.74	50.57	40.60	33.62	42.48	52.40	42.83
Color	2.96	5.03	8.39	5.46	3.68	5.75	9.50	6.31
Texture	2.83	4.92	7.88	5.21	3.45	5.57	9.28	6.10